NASA Technical Paper 1573

Fabrication and Evaluation of Brazed Titanium-Clad Borsic®/Aluminum Compression Panels

Dick M. Royster, Robert R. McWithey,
and Thomas T. Bales

MARCH 1980

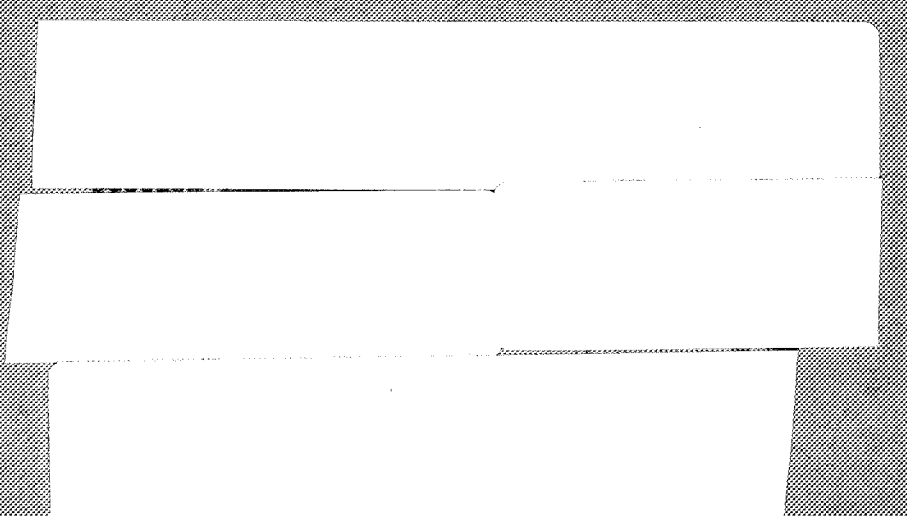

NASA

NASA Technical Paper 1573

Fabrication and Evaluation of Brazed Titanium-Clad Borsic®/Aluminum Compression Panels

Dick M. Royster, Robert R. McWithey,
and Thomas T. Bales
Langley Research Center
Hampton, Virginia

National Aeronautics
and Space Administration

**Scientific and Technical
Information Office**

1980

SUMMARY

Methods for fabricating and joining metal-matrix composites have been studied at the NASA Langley Research Center. These studies have led to the development of a hybrid composite material consisting of a high-strength Borsic[1]/aluminum core with ductile titanium-foil outer surfaces. The present study was conducted to determine the tensile strength of titanium-clad Borsic/aluminum sheet material and to fabricate and evaluate the compressive properties of titanium-clad Borsic/aluminum skin-stiffened panels. Panel skins and stringers were joined by brazing and were tested in axial compression at room and elevated temperatures. Titanium cladding on the surfaces of the Borsic/aluminum serves as a diffusion barrier between the matrix and braze alloy which alleviates fiber and matrix degradation during brazing. The test results show that titanium-clad Borsic/aluminum unidirectional sheet materials had longitudinal and transverse tensile strengths that were 0.9 and 2.5 times, respectively, that of unclad Borsic/aluminum unidirectional sheet materials. Specific buckling strengths were higher for the titanium-clad Borsic/aluminum skin-stringer panels than for similar unclad Borsic/aluminum panels. Buckling loads calculated with a finite-element analysis were in good agreement with experimentally determined buckling loads.

INTRODUCTION

Methods for fabricating and joining boron/aluminum (B/Al) and Borsic/aluminum (Bsc/Al) composite materials have been studied at NASA Langley Research Center (LaRC) and are reported in reference 1. The brazing study from reference 1 showed that interaction between the braze alloy and the composite during brazing reduced both matrix and fiber strengths. Other studies (refs. 2 and 3) have shown that Bsc/Al can be brazed successfully with a minimum of fiber and matrix degradation by adding a thin outer layer of 1100 aluminum alloy to serve as a diffusion barrier between the braze alloy and the composite.

Further brazing studies have led to the development of a hybrid composite which consists of a high strength Bsc/Al core with ductile titanium-foil outer surfaces. This material is identified in this report as titanium-clad Borsic/aluminum (Ticlad Bsc/Al). The titanium cladding on the surfaces of the Bsc/Al serves as a diffusion barrier to alleviate fiber and matrix degradation during brazing and also provides a durable outer surface. A study was initiated to determine the tensile strength of Ticlad Bsc/Al sheet material and to fabricate and evaluate the compressive properties of Ticlad Bsc/Al skin-stiffened panels. The skins and stringers were joined by brazing and were tested in axial compres-

---

[1]Borsic: Registered trade name of United Aircraft Products, Inc.

sion at room and elevated temperatures. Brazing parameters were established by brazing and testing double-overlap tensile specimens. The data from the panel tests include buckling strength and failure strength. Buckling strengths calculated with a finite-element analysis were compared with the experimental values. Sections of the tested panels were examined metallurgically, and fiber bend tests were made to demonstrate the effectiveness of the titanium foil as a diffusion barrier between the braze alloy and the aluminum matrix.

The physical quantities defined in this paper are given both in the International System of Units (SI) and in U.S. Customary Units. Measurements and calculations were made in the U.S. Customary Units.

The VIPASA computer analysis described in the appendix was performed by Gerald G. Weaver, graduate student at the University of Delaware.

Use of trade names or names of manufacturers in this report does not constitute an official endorsement of such products or manufacturers, either expressed or implied, by the National Aeronautics and Space Administration.

SPECIMEN FABRICATION

Material

The titanium-clad Borsic/aluminum (Ticlad Bsc/Al) sheet (or skin) material used in this investigation was obtained from one source. The material consisted of Ti-75A foil outer layers 0.15 mm (0.006 in.) thick and six plies of Borsic fibers 0.145 mm (0.0057 in.) in diameter aligned unidirectionally in a 6061 aluminum alloy matrix. (See fig. 1.) The nominal fiber-volume fraction of the composite material was 0.48; the nominal total sheet thickness was 1.35 mm (0.053 in.). The titanium foil and individual Bsc/Al plies were stacked together and consolidated in one operation by diffusion bonding at 800 K (975° F) and 31 MPa (4500 psi) pressure for 5 hours. These values for the consolidation parameters are the same as those required to consolidate Bsc/Al sheets. A cross section of the consolidated sheet material is shown in figure 2.

Test Specimens

Tension.- Schematic diagrams of the test specimens used to determine the tensile strength of the Ticlad Bsc/Al material and tensile shear strength of brazed joints are shown in figure 3. The tensile specimens (fig. 3(a)) were cut to size by shearing; the Borsic fibers were either aligned with the specimen length (longitudinal) or aligned perpendicular to the specimen length (transverse). The double-overlap braze joint specimens (fig. 3(b)) were electron discharge machined from panels consisting of two sheets of Ti-6Al-4V titanium alloy brazed to two Ticlad Bsc/Al strips 25.4 mm (1.0 in.) wide. The overlap for the brazed specimens was 3.05 mm (0.12 in.). The specimens were

brazed with 4047 aluminum alloy brazing foil (AWS-ASTM-BALSi-4)[2] using the parameters established in reference 2.

Compression.- The three skin-stringer panel configurations which were used for the Ticlad Bsc/Al axial compression tests are shown in figure 4. Two configurations used hat-shaped stringers identified as large stringer (L) and small stringer (S). Stringers of these two configurations were supplied by a commercial source. The only difference in the hat-shaped stringers, other than size, was that the titanium cladding was 0.15 mm (0.006 in.) thick on the large stringers and 0.075 mm (0.003 in.) thick on the small stringers. The nominal sheet thicknesses of the large and small stringers were 1.35 mm (0.053 in.) and 1.20 mm (0.047 in.), respectively. The filament orientation in the stringers was always in the longitudinal direction.

The hat-shaped stringers were fabricated from consolidated Ticlad Bsc/Al flat sheet by a hot forming process. During the forming, a stainless steel caul sheet 0.81 mm (0.032 in.) thick was positioned on the tension surface of the Ticlad Bsc/Al sheet to help prevent crack occurrence in the bend of the stringers. Production of each hat-shaped stringer required four separate forming operations, one for each bend, with the caul sheet shifted to the tension side for each bend. Each bend was formed in a heated die after the caul sheet and Ticlad Bsc/Al material were exposed to the forming temperature of 730 K (850° F) for 6 minutes. A high-temperature lubricant was used to prevent interaction or bonding of the stringer to the die. Final sizing of the stringer was performed in a hot sizing fixture to ensure that the stringer elements would be straight.

In the third panel configuration, designated H in figure 4, the stringer consisted of a Ti-3Al-2.5V titanium alloy honeycomb core brazed to a Ticlad Bsc/Al cap using 4047 aluminum alloy brazing foil. Panels of this configuration were fabricated at LaRC. The nominal densities of the titanium alloy honeycomb core were 112 kg/m^3 (7 lbm/ft^3) and 208 kg/m^3 (13 lbm/ft^3).

The cross sections of the skin-stringer panels used in the investigation are shown in figure 5; the dimensions and mass of each panel are listed in table I. The skins were joined to the hat-shaped stringers and honeycomb-core stringers by brazing. The filaments in the skins and caps were always oriented in the longitudinal direction. The nominal thickness of all the skins was 1.35 mm (0.053 in.).

The dimensions of the large stringers were made identical with those of the stringers described in reference 1. The small stringers were designed for use on a stiffened panel using design conditions presented in reference 3. The honeycomb-core stringer was designed to gain experience with farbicating and testing panels of this configuration. Geometrically identical laminates

---

[2]Available commercially as Alcoa No. 718 brazing sheet from Aluminum Company of America.

were used to form the skin of the three panel configurations. The panels were also designed to force the lowest buckling mode to occur as a local mode in the skin.

Brazing Methods

Hat-shaped skin-stringer panels.- The Ticlad Bsc/Al hat-shaped stringers were supplied in lengths of 259.1 mm (10.2 in.). The Ticlad Bsc/Al skin material was supplied in sheets 760 mm by 500 mm (30 in. by 20 in.) which were cut to 259.1 mm by 152.4 mm (10.2 in. by 6.0 in.) for the large hat-shaped stringers and to 259.1 mm by 111.8 mm (10.2 in. by 4.4 in.) for the small hat-shaped stringers. The skin material was cut with a conventional diamond-wheel saw. Prior to brazing, the skins and stringers were chemically cleaned.

The Ticlad Bsc/Al stringers were brazed to Ticlad Bsc/Al skins with 4047 aluminum alloy brazing foil 0.075 mm (0.003 in.) thick. A cross section of the tooling for brazing the panels is shown in figure 6. The basic joining fixture used titanium honeycomb-core tooling. Pressure was applied to the joint by a stainless steel, inflatable diaphragm located on top of the brazing pack. The stringer and skin were assembled with the brazing alloy foil positioned between the mating surfaces. Alignment of stringer and skin was maintained during initial assembly by small tack welds located at the ends of the stringer flanges. Panels were brazed in a vacuum furnace at 870 K (1100° F) for 5 minutes. A pressure of approximately 14 kPa (2 psi) was maintained during brazing by inflating the stainless steel diaphragm.

Honeycomb-core skin-stringer panels.- The honeycomb-core skin-stringer panels were fabricated in a two-step brazing process. In the first step, the titanium honeycomb core was brazed to the Ticlad Bsc/Al cap material using 4047 aluminum brazing foil 0.25 mm (0.010 in.) thick. Brazing was accomplished at 870 K (1100° F) for 5 minutes in a vacuum furnace. Following brazing, the capped honeycomb core was electron discharge machined to the nominal stringer size of 59.7 mm by 39.4 mm (2.35 in. by 1.55 in.). After vapor degreasing of the parts, the capped honeycomb-core stringers were brazed to the Ticlad Bsc/Al skin material to complete the second step. A similar joining fixture was used as in brazing the hat-shaped skin-stringer panels. Brazing was accomplished at 870 K (1100° F) in a vacuum for 5 minutes using 4047 aluminum alloy brazing foil 0.25 mm (0.010 in.) thick.

TESTS

Tension

The longitudinal and transverse tensile specimens and the double-overlap braze joint specimens were tested at room temperature using a screw-driven testing machine of 45-kN (10-kip) capacity at a cross-head speed of 1.27 mm/min (0.05 in./min). The tests were terminated upon fracture of the specimens. Failure loads were recorded from the dial of the test machine.

Compression

Following fabrication, the ends of each panel were "potted" with a room-temperature-curing epoxy for the room-temperature tests and an elevated-temperature-curing epoxy for the elevated-temperature tests. Potting facilitated machining the panel ends parallel and to test length. This treatment also prevented crushing or "brooming" of the panel ends during the tests. The skins were clamped against a flat plate, and the ends of the panels were machined flat and parallel to each other and perpendicular to the longitudinal axis of the panels. To ensure uniform loading through the panel, the ends of each panel were checked, after machining, for parallelism and flatness by placing the panel between parallel heads of a test machine, applying a small load, and inserting a feeler gage between each head and the machine ends of the panel. The tolerance between the ends of the machined panel and the heads of the test machine were within 0.05 mm (0.002 in.) for all the panels.

Each panel was instrumented with strain gages on the skin and stringer, and thermocouples were spot welded to those panels tested at elevated temperature. (See fig. 7.) Linear variable differential transducers (LVDT) were used to measure panel shortening. The room-temperature test setup for the panels is shown in figure 8. For the elevated-temperature tests, the specimens were heated from both the skin and stringer sides with removable quartz-lamp radiators. The unloaded edges of the panels were simply supported with knife edges positioned 6.35 mm (0.25 in.) from each panel edge. Outputs from strain gages, thermocouples, LVDT's, and the load indicator were recorded during the tests.

A preload of 4.5 kN (1.0 kip) was applied to check the recording system. The panels were then loaded at room temperature to failure at a rate of approximately 45 kN/min (10 kips/min). Data were recorded every 10 seconds until local buckling was detected and every second thereafter to failure.

The elevated-temperature tests were conducted at 505 K (450° F). The panels were heated to 505 K (450° F) and the temperature was allowed to stabilize prior to testing. Thermocouple readings indicated that the skins and crown of the stringers were within 3 K (5° F) of the test temperature. After the strain gages were zeroed, the heads of the test machine were brought into contact with the panels and the tests were conducted in the same fashion as those at room temperature.

Metallurgical Investigation

Samples were cut from undeformed regions of the tested panels for metallographic examination of representative cross sections. The samples were mounted in phenolic resin, polished, and examined with a metallograph. The photomicrographs were studied to determine the quality of the joints and to identify metallurgical changes in the material resulting from fabrication.

RESULTS AND DISCUSSION

Tensile Tests

Results of tests on the Ticlad Bsc/Al tensile specimens are listed in table II. The longitudinal tensile strength varied from about 1032 MPa (150 ksi) to 1247 MPa (181 ksi) with an average of about 1172 MPa (170 ksi). The average is very close to the rule-of-mixtures value of 1138 MPa (165 ksi) obtained by using tensile strengths of 1310 MPa (190 ksi) and 552 MPa (80 ksi) for Bsc/Al and Ti-75A, respectively. The average longitudinal strength of the Ticlad Bsc/Al was thus about 10 percent less than that of Bsc/Al. The average transverse tensile strength of the Ticlad Bsc/Al, on the other hand, was approximately 338 MPa (49 ksi), which is about 2.5 times that of unidirectional Bsc/Al and about 40 percent greater than predicted by the rule of mixtures.

The results of the tests on the double-overlap braze joint specimens are listed in table III. The average maximum joint strength of about 110 MPa (16 ksi) agrees with data obtained from similar braze joint tests on Bsc/Al in reference 2. The test results of the double-overlap braze joint specimens verify that the brazing parameters of this study are adequate for the brazing of the skin-stringer panels.

Panel Compression Tests

The results from the axial compression tests are presented in figures 9 to 12 and in table IV. Typical LVDT load-shortening curves for the three skin-stringer panel configurations tested are shown in figure 9. All load-shortening curves for a given test temperature and stringer configuration are similar. The curves illustrate the lower strength and stiffness of the panels tested at 505 K (450° F). The average strain at the onset of local elastic buckling, as indicated by strain reversal, is plotted on the curves as $\bar{\varepsilon}$ (listed in table IV for all the panels) at the load corresponding to strain reversal. The skin-stringer panels withstood 15 to 40 percent more compressive load following buckling and prior to failure. Failure occurred by simultaneous crippling of the stringer and skin. By comparison, the Bsc/Al panels in reference 1 often exhibited buckling and failure simultaneously.

The compressive stress-strain curves of Ticlad Bsc/Al at room temperature and 505 K (450° F) are shown in figure 10. The data plotted are from strain gages located on the skin of the panels. Only the linear portions of the stress-strain curves are plotted with the curves terminated prior to panel buckling. The value of Young's modulus for the Ticlad Bsc/Al at room temperature was 213.7 GPa 31.0 × 10^6 psi), which is very close to the rule-of-mixtures value of 217 GPa (31.5 × 10^6 psi) obtained when using a modulus of 248 GPa (36 × 10^6 psi) for the Bsc/Al and 110 GPa (16 × 10^6 psi) for the Ti-75A. Young's modulus of the Ticlad Bsc/Al at 505 K (450° F) was 175.8 GPa (25.5 × 10^6 psi), about 17 percent less than that at room temperature.

Buckling strength.- The buckling strength is defined as the buckling load of the panel divided by the cross-sectional area of the panel as given in

table I. Comparisons between experimental and analytical buckling strengths are presented in figure 11. The analytical buckling strengths were determined using the VIPASA computer program described in reference 4; a detailed explanation of the analytical procedure is presented in the appendix. The circular symbol in figure 11 indicates the average buckling strength of three duplicate panels, and the vertical bars represent the scatter in the experimental results. The ratio b/t_s on the abscissa is the width of unsupported skin b divided by the skin thickness t_s. The dimensions b and t_s are illustrated in figure 11 for the panel configurations. The ratio b/t_s of the skin was chosen as an appropriate parameter because buckling initially occurs in the skin for all panels.

Excellent agreement between analytical and experimental buckling strengths was obtained for the panels with the large hat-shaped stringer; somewhat poorer agreement was obtained for the other configurations. The data show that the elevated temperature reduced the buckling strengths by 9 to 17 percent.

The agreement between present analytically and experimentally determined buckling strengths for the panels with hat-shaped stringers shown in figure 11 is much better than the agreement between similar data given in reference 1. To determine whether differences in the analytical programs accounted for the good agreement in the present analysis, the VIPASA program was used to determine buckling loads and modes for several of the configurations given in reference 1. The VIPASA results were in agreement with the analytical results from reference 1; and, therefore, the good agreement in the present study is the result of changes in panel buckling behavior.

In the previous study (ref. 1), poor agreement between analytical and experimental results was attributed to a local decrease in transverse Young's modulus of the Bsc/Al which was the result of local bending strains. In the present study, several factors preclude this reduction in transverse modulus. Examination of the mode shapes indicates that for a given out-of-plane skin deformation, lower bending strains are present in the cross section of the present panels. Titanium cladding also reduces transverse bending strains in the Bsc/Al, because only the titanium cladding experiences the maximum "outer-fiber" strains caused by bending. Both factors allow the initial Bsc/Al transverse modulus 131.0 GPa (19×10^6 psi), which was used in both analyses (ref. 1 and present), to be more effective in resisting buckling in the present panels.

Failure strength.- The average failure strength of the skin-stringer panels is plotted against the ratio b/t_s in figure 12. The average failure strength is defined as the maximum compressive load applied to the panel divided by the cross-sectional area of the panel as given in table I. Scatter in the data is indicated by the vertical bars in the figure. The elevated temperature reduced the strength by 8 to 14 percent.

Specific buckling strength.- The specific buckling strength of the panels is defined as the panel buckling strength divided by the panel density. Panel density was determined by dividing the mass of the panel by both the panel cross-sectional area (excluding the honeycomb-core area) and the panel length (see table I). Figure 13 presents the specific buckling strength plotted

against b/t_s for the panels in the present study and for panels (from refs. 1 and 5) with similar configurations. The densities of the panel material in the present study and the panel material from the references are given in the following table:

Material	Density	
	kg/m^3	lbm/in^3
Ticlad Bsc/Al:		
0.075 mm (0.003 in.) cladding	2900	0.105
0.15 mm (0.006 in.) cladding	3100	.112
Bsc/Al (ref. 1)	2700	.097
Ti-6Al-4V (ref. 5)	4400	.16

These densities indicate that titanium cladding does not appreciably change panel density from that for an all Bsc/Al panel. Panel buckling characteristics do differ, however, and some of these differences are discussed in the appendix.

The data in figure 13 show that the specific buckling strengths of the Ticlad Bsc/Al panels were 1.5 to 1.7 times those of similar Bsc/Al panels in reference 1 and titanium weld-braze panels in reference 5. The improvement in the specific buckling strengths of the skin-stringer panels in the present study relative to the brazed Bsc/Al panels of reference 1 is attributed to reduced transverse bending strains in the present panels resulting from changes in the buckling mode shapes and to the effects of the titanium cladding, as discussed previously in the section "Buckling strength." The improvement in the specific buckling strengths of the panels in the present study compared with the specific strengths of the titanium weld-braze panels of reference 5 is due to the higher transverse stiffness as well as the lower densities of the present panels. The results indicate that the panels with honeycomb-core stringers have a lower specific buckling strength than the Ticlad Bsc/Al panels with hat-shaped stringers. However, the honeycomb-core stringers provide considerable local stability to the skin and offer simplified manufacturing processes that warrant further investigation for use in compression panels.

Failures.- Typical failures of the panels tested in axial compression are shown in figure 14. The panel failures were the same for tests at both room temperature and 505 K (450° F). All panels exhibited local buckling prior to simultaneous crippling of the stringer and skin. Panels with the hat-shaped stringers (figs. 14(a) and 14(b)) exhibited transverse fractures of the Ticlad Bsc/Al material in the stringer and skin across the center of the panels. There were no braze-joint failures. The panels with the honeycomb-core stringer exhibited transverse fractures of the skin and some braze-joint fractures between the skin and honeycomb-core stringer associated with the buckle pattern (fig. 14(c)). The Ticlad Bsc/Al cap material buckled but did not fracture or separate from the honeycomb core.

Metallurgical investigation.- The braze joints shown in figure 15 are typical for all the panels with hat-shaped stringers. The effectiveness of the Ti-75A foil as a diffusion barrier is seen by the absence of silicon particles in the adjacent matrix material. On the whole, silicon diffusing into the 6061 aluminum matrix embrittles the matrix and reduces the strength of both filaments and matrix (ref. 1). There was also no evidence of either titanium or Bsc/Al delaminations.

The braze joints in figure 16 are typical for all the panels with honeycomb-core stringers. The photomicrograph showing the braze joint between the honeycomb core and skin (fig. 16(a)) shows less braze filleting than between the honeycomb core and cap (fig. 16(b)). Because some braze material fractured between the skin and honeycomb core at panel failure, but did not fracture between the honeycomb core and cap, braze filleting on the skin side appears to have been marginal. The titanium cladding also prevented filament damage because the titanium honeycomb core was not forced through the titanium cladding during the brazing operation, a phenomenon which frequently occurs in pack brazing of aluminum matrix composites and honeycomb materials.

Fiber Strength

To determine the effects of the brazing process on the Borsic fibers, the strengths of fibers leached from "as received" skin material and "as fabricated" stringers were compared with the strengths of fibers leached from samples cut from brazed and tested panels. The skin and stringer samples were cut from the brazed panels in areas not associated with panel failure. Fiber strengths were determined by bend tests as described in reference 2. Approximately 40 fibers from each skin and stringer were tested.

The strengths of the fibers from each of the brazed panels (either skin or stringer) ranged from 3.10 to 3.80 GPa (450 to 550 ksi); the average strength for each panel was between 3.60 and 3.70 GPa (520 and 540 ksi). The fiber strengths of the "as received" skin material and the "as fabricated" stringers were within the same range. Therefore, the skin and stringer fibers appear to have been unaffected by the temperatures associated with stringer fabrication or with panel brazing. On the basis of these results, brazing is considered to be a viable means of joining Ticlad Bsc/Al.

Application

At LaRC, the fabrication, joining, and testing of metal-matrix composites have led to the incorporation of these materials into flight hardware for supersonic aircraft. In reference 3 a full-scale structural panel with a Bsc/Al skin and a titanium honeycomb core was successfully designed, fabricated, and tested to meet the requirements of an upper wing panel for the YF-12 aircraft. The current characterization program on Ticlad Bsc/Al material has led to the design and fabrication of a panel composed of Ti-3Al-2.5V honeycomb-core stringers brazed to a Ticlad Bsc/Al skin and cap, as shown in figure 17. Preliminary data (ref. 6) show that the panel has successfully met the strength and stiffness requirements for flight service on the YF-12 aircraft at Mach 3.

CONCLUDING REMARKS

An investigation has been conducted to determine the compressive properties of titanium-clad Borsic/aluminum skin-stringer, structural components fabricated by brazing. The following results have been found:

1. Titanium-clad Borsic/aluminum unidirectional sheet materials had longitudinal and transverse tensile strengths that were 0.9 and 2.5 times, respectively, that of unclad Borsic/aluminum unidirectional sheet materials.

2. Following local skin buckling, the titanium-clad Borsic/aluminum panels withstood from 15 to 40 percent more compressive load prior to failure, whereas the unclad Borsic/aluminum panels studied in NASA TP-1121 often exhibited buckling and failure simultaneously.

3. Specific buckling strengths for the titanium-clad Borsic/aluminum skin-stringer panels were 1.5 to 1.7 times those for similar unclad Borsic/aluminum panels studied in NASA TP-1121 and titanium weld-braze panels studied in NASA TN D-7281.

4. Good agreement was shown between experimental buckling loads and those analytically predicted by the VIPASA program.

5. Compression tests of the hat-stiffened panels and metallurgical investigation of the joints after panel failure indicated no failures in the braze joints.

6. Titanium cladding provides an effective diffusion barrier between the braze alloy and the 6061 aluminum-alloy-matrix material.

7. Borsic fiber strengths were unaffected by the stringer fabrication and brazing processes.

8. Results from the current study have led to the successful design, fabrication, and testing of a full-scale wing panel for flight testing on the YF-12 aircraft at Mach 3.

Langley Research Center
National Aeronautics and Space Administration
Hampton, VA 23665
November 16, 1979

APPENDIX

PANEL BUCKLING ANALYSIS

The VIPASA computer program (ref. 4) was used to calculate critical buckling loads and mode shapes for each of the skin-stringer panel configurations discussed in the present study. The VIPASA models used in the analyses are shown in figure 18. Each model consisted of an assembly of balanced and symmetric flat-plate elements simply supported near the edges of the skin. These boundary conditions are consistent with the panel test conditions. In the panel model with hat-shaped stringers, each brazed joint between the stringer and skin was modeled using eight flat-plate elements. The adjacent edges of these eight elements were rigidly linked together, thus providing a good approximation to the actual physical joints. The honeycomb-core stringer was modeled as a single plate element; the element included the skin over the honeycomb core, the honeycomb core, and the cap. In this panel model, deformation compatibility was maintained across the skin of the panel. Out-of-plane shear deformations of the honeycomb core are not considered in the VIPASA program.

Differences exist between the VIPASA models and the test panels at the loaded ends. Whereas the VIPASA program calculates buckling load and modes with simple supports at the loaded ends, the test panel ends were embedded in potting compound that produced end boundary conditions nearly equivalent to fixed ends. However, because the longitudinal buckling half-wavelengths of the panels are short, the proper buckling loads and mode shapes were obtained from the VIPASA analyses despite the differences in end boundary conditions. The differences in the loaded end boundary conditions would not significantly affect analytical buckling load and mode results unless the specimen length in the analysis is either reduced to values less than the length of the critical buckling half-wavelength, or is increased to a value that allows Euler column buckling.

In operating the VIPASA program, the user must input all dimensions for each unique plate element, define the shape of the panel cross section, and provide a list of half-wavelengths to be examined. In addition, appropriate material properties (see table V) must be supplied to the program. The program generates a stiffness matrix for each element from which a total stiffness matrix is formed for the structure. The program then solves the buckling eigenvalue problem for each half-wavelength requested by the user.

Typical mode shape results from the VIPASA analyses are shown in figure 19 for the two basic panel configurations. In both the small-hat and large-hat configurations (fig. 19(a)), very little deformation is apparent in the stiffener cross section, whereas the skin over the hat exhibits significant out-of-plane deformation. This analytical result is consistent with strain-gage data from the panels, which indicated that initial buckling occurred in this section of skin. Post-failure examination of the skin indicated half-wavelengths nearly equal to those given by the VIPASA analysis. The mode shape for the panel with honeycomb-core stringer (fig. 19(b)) indicates that buckling deformation occurs only in the outer skin portions of the panel in a nonsymmetrical pattern. This pattern was also observed in post-failure examination of the panels.

REFERENCES

1. Royster, Dick M.; Wiant, H. Ross; and McWithey, Robert R.: Effects of Fabrication and Joining Processes on Compressive Strength of Boron/Aluminum and Borsic/Aluminum Structural Panels. NASA TP-1121, 1978.

2. Royster, Dick M.; Wiant, H. Ross; and Bales, Thomas T.: Joining and Fabrication of Metal-Matrix Composite Materials. NASA TM X-3282, 1975.

3. Bales, Thomas T.; Wiant, H. Ross; and Royster, Dick M.: Brazed Borsic/Aluminum Structural Panels. NASA TM X-3432, 1977.

4. Wittrick, W. H.; and Williams, F. W.: Buckling and Vibration of Anisotropic or Isotropic Plate Assemblies Under Combined Loadings. Int. J. Mech. Sci., vol. 16, no. 4, Apr. 1974, pp. 209-239.

5. Bales, Thomas T.; Royster, Dick M.; and Arnold, Winfrey E., Jr.: Development of the Weld-Braze Joining Process. NASA TN D-7281, 1973.

6. Hoffman, Edward L.; Bales, Thomas T.; and Payne, Lee: Fabrication Research for Supersonic Cruise Aircraft. The Enigma of the Eighties: Environment, Economics, Energy, Volume 24 of National SAMPE Symposium and Exhibition, Book 1, Soc. Advance. Mater. & Process Eng., c.1979, pp. 232-241.

TABLE I.- DIMENSIONS OF SKIN-STRINGER PANELS

(a) SI Units

Panel	Length, mm	W, mm	Mass, kg	Area, cm^2	w, mm	b_h, mm	b_f, mm	b_w, mm	r_a, mm	t_w, mm	t_s, mm
1S	259.1	111.8	0.220	2.82	99.1	28.7	23.1	25.9	7.92	1.212	1.359
2S	↓	↓	.217	2.79	↓	28.2	23.1	25.9	↓	1.209	1.331
3S			.215	2.77		29.5	22.6	25.4		1.201	1.331
4S			.216	2.78		29.0	22.9	25.7		1.214	1.331
5S			.215	2.76		29.0	22.1	28.2		1.199	1.328
6S			.219	2.81		29.1	21.8	26.9		1.204	1.341
1L	259.1	152.4	0.349	4.35	139.7	41.4	31.8	38.6	6.35	1.372	1.359
2L	↓	↓	.342	4.30	↓	42.4	31.5	38.6	↓	1.359	1.346
3L			.355	4.43		43.2	32.0	38.6		1.374	1.369
4L			.349	4.36		41.7	31.8	38.6		1.377	1.356
5L			.337	4.21		41.7	29.7	39.1		1.351	1.364
6L			.329	4.12		41.9	30.0	37.8		1.344	1.341
									Density of core, kg/m^3	t_c, mm	
1H	251.5	152.4	0.401	2.89	139.7	59.7		39.1	208.2	1.384	1.354
2H	↓	↓	.395	2.90	↓	↓		39.1	208.2	1.384	1.354
3H			.349	2.92				40.4	112.1	1.354	1.384
4H			.402	2.92				39.1	208.2	1.384	1.369
5H			.395	2.91				39.1	208.2	1.384	1.356
6H			.402	2.90				39.1	208.2	1.384	1.379
7H			.351	2.93				40.4	112.1	1.369	1.374

TABLE I.- Concluded

(b) U.S. Customary Units

Panel	Length, in.	W, in.	Mass, lbm	Area, in^2	w, in.	b_h, in.	b_f, in.	b_w, in.	r_a, in.	t_w, in.	t_s, in.
1S	10.2	4.4	0.484	0.437	3.9	1.13	0.91	1.02	0.312	0.0477	0.0535
2S	↓	↓	.479	.433	↓	1.11	.91	1.02	.312	.0476	.0524
3S	↓	↓	.475	.430	↓	1.16	.89	1.00	.312	.0473	.0524
4S	↓	↓	.477	.431	↓	1.14	.90	1.01	.312	.0478	.0524
5S	↓	↓	.475	.428	↓	1.14	.87	1.11	.312	.0472	.0523
6S	↓	↓	.482	.436	↓	1.15	.86	1.06	.312	.0474	.0528
1L	10.2	6.0	0.769	0.674	5.5	1.63	1.25	1.52	0.250	0.0540	0.0535
2L	↓	↓	.755	.666	↓	1.66	1.24	1.52	.250	.0535	.0530
3L	↓	↓	.783	.686	↓	1.70	1.26	1.52	.250	.0541	.0539
4L	↓	↓	.769	.676	↓	1.64	1.25	1.52	.250	.0542	.0534
5L	↓	↓	.743	.653	↓	1.64	1.17	1.54	.250	.0532	.0537
6L	↓	↓	.726	.638	↓	1.65	1.18	1.49	.250	.0529	.0528
									Density of core, lbm/ft^3	t_c, in.	
1H	9.9	6.0	0.885	0.448	5.5	2.35		1.54	13	0.0545	0.0533
2H	↓	↓	.870	.449	↓	↓		1.54	13	.0545	.0533
3H	↓	↓	.769	.452	↓	↓		1.59	7	.0533	.0545
4H	↓	↓	.887	.452	↓	↓		1.54	13	.0545	.0539
5H	↓	↓	.870	.451	↓	↓		1.54	13	.0545	.0534
6H	↓	↓	.887	.450	↓	↓		1.54	13	.0545	.0543
7H	↓	↓	.774	.454	↓	↓		1.59	7	.0539	.0541

TABLE II.- TENSILE TEST DATA FOR TITANIUM-CLAD

BORSIC/ALUMINUM MATERIAL

Specimen	Area		Failure load		Failure stress	
	cm^2	in^2	kN	lbf	MPa	ksi
Longitudinal direction						
1	0.1787	0.0277	20.6	4640	1154.9	167.5
2	.1768	.0274	18.2	4100	1031.5	149.6
3	.1800	.0279	22.1	4975	1230.1	178.4
4	.1781	.0276	21.7	4875	1217.7	176.6
5	.1748	.0271	20.5	4600	1169.4	169.6
6	.1748	.0271	19.8	4450	1133.5	164.4
7	.1716	.0266	20.5	4600	1192.8	173.0
8	.1748	.0271	21.8	4900	1247.3	180.9
Transverse direction						
1	0.2780	0.0431	10.0	2250	359.9	52.2
2	.2864	.0444	10.3	2325	360.6	52.3
3	.2877	.0446	10.8	2425	375.8	54.5
4	.2832	.0439	10.4	2340	367.5	53.3
5	.2858	.0443	10.5	2360	367.5	53.3
6	.2845	.0441	9.9	2240	350.3	50.8
7	.2851	.0442	9.6	2170	338.5	49.1
8	.2851	.0442	9.7	2175	339.2	49.2
9	.2729	.0423	9.6	2150	350.3	50.8
10	.3406	.0528	11.2	2515	328.2	47.6
11	.3367	.0522	11.1	2495	329.6	47.8
12	.2368	.0367	7.5	1690	317.9	46.1
13	.1619	.0251	5.1	1140	313.0	45.4
14	.1626	.0252	5.0	1115	304.8	44.2
15	.1658	.0257	5.0	1120	300.0	43.5

TABLE III.- TENSILE SHEAR STRENGTH TEST DATA

FOR DOUBLE-OVERLAP BRAZED SPECIMENS

Specimen	Area		Failure load		Failure stress	
	cm^2	in^2	kN	lbf	MPa	ksi
1	1.628	0.2524	18.5	4160	113.8	16.5
2	↓	↓	18.8	4225	115.1	16.7
3			17.5	3940	107.6	15.6
4			18.4	4140	113.1	16.4
5			15.6	3500	95.8	13.9
6			18.0	4050	113.1	16.4
7			15.3	3450	94.5	13.7
8			19.0	4275	116.5	16.9
9			18.0	4240	115.8	16.8
10			18.3	4125	112.4	16.3
11			18.8	4225	115.1	16.7
12			18.1	4075	111.0	16.1
13			17.2	3875	106.2	15.4
14			18.0	4050	110.3	16.0

TABLE IV.- AXIAL COMPRESSION DATA FROM

SKIN-STRINGER PANELS

(a) SI Units

Panel	Maximum load, kN	Average maximum stress, MPa	Buckling load, kN	Average buckling stress, MPa	Average strain at buckling, $\bar{\varepsilon}$, mm/mm
Room temperature					
4S	255.4	918.4	194.9	700.5	0.00314
5S	262.6	950.8	190.6	690.2	.00318
6S	269.7	959.1	209.5	744.7	.00350
505 K					
1S	224.6	796.4	169.2	599.9	0.00322
2S	227.1	812.9	177.7	636.4	.00327
3S	242.3	871.6	176.3	635.7	.00340
Room temperature					
1L	306.4	704.7	236.5	544.0	0.00249
2L	289.0	673.0	242.1	563.3	.00259
3L	286.5	647.4	227.7	514.4	.00257
505 K					
4L	257.9	591.6	203.5	466.8	0.00251
5L	269.5	639.9	156.7	371.6	.00173
6L	257.0	624.7	190.9	462.0	.00263
Room temperature					
1H	243.5	842.6	176.3	610.2	0.00307
2H	226.3	781.2	146.6	506.1	.00232
3H	239.4	821.2	146.6	502.6	.00246
4H	230.7	791.5	143.3	491.6	.00233
505 K					
5H	201.4	692.3	149.9	515.1	0.00277
6H	216.9	746.7	141.2	486.8	.00272
7H	188.7	644.0	123.3	421.3	.00218

TABLE IV.- Concluded

(b) U.S. Customary Units

Panel	Maximum load, lbf	Average maximum stress, ksi	Buckling load, lbf	Average buckling stress, ksi	Average strain at buckling, $\bar{\varepsilon}$, in./in.
Room temperature					
4S	57 428	133.2	43 809	101.6	0.00314
5S	59 033	137.9	42 854	100.1	.00318
6S	60 638	139.1	47 105	108.0	.00350
450° F					
1S	50 488	115.5	38 040	87.0	0.00322
2S	51 052	117.9	39 948	92.3	.00327
3S	54 479	126.7	39 645	92.2	.00340
Room temperature					
1L	68 879	102.2	53 178	78.9	0.00249
2L	64 976	97.6	54 435	81.7	.00259
3L	64 412	93.9	51 182	74.6	.00257
450° F					
4L	57 992	85.8	45 761	67.7	0.00251
5L	60 595	92.8	35 220	53.9	.00173
6L	57 775	90.6	42 724	67.0	.00263
Room temperature					
1H	54 739	122.2	39 645	88.5	0.00307
2H	50 879	113.3	32 965	73.4	.00232
3H	53 828	119.1	32 965	72.9	.00246
4H	51 876	114.8	32 228	71.3	.00233
450° F					
5H	45 283	100.4	33 702	74.7	0.00277
6H	48 753	108.3	31 750	70.6	.00272
7H	42 421	93.4	27 717	61.1	.00218

TABLE V.- VIPASA MATERIAL PROPERTY INPUTS

Borsic/aluminum at room temperature:	
Young's modulus - longitudinal direction, GPa (psi)	227.5 (33 × 10^6)
Young's modulus - transverse direction, GPa (psi)	131.0 (19 × 10^6)
Shear modulus, GPa (psi)	57.2 (8.3 × 10^6)
Major Poisson's ratio	0.26
Borsic/aluminum at 505 K (450° F):	
Young's modulus - longitudinal direction, GPa (psi)	200.0 (29 × 10^6)
Young's modulus - transverse direction, GPa (psi)	96.5 (14 × 10^6)
Shear modulus, GPa (psi)	51.7 (7.5 × 10^6)
Major Poisson's ratio	0.26
Ti-75A cladding at room temperature:	
Young's modulus, GPa (psi)	110.3 (16 × 10^6)
Shear modulus, GPa (psi)	44.8 (6.5 × 10^6)
Poisson's ratio	0.34
Ti-75A cladding at 505 K (450° F):	
Young's modulus, GPa (psi)	96.5 (14 × 10^6)
Shear modulus, GPa (psi)	40.0 (5.8 × 10^6)
Poisson's ratio	0.34

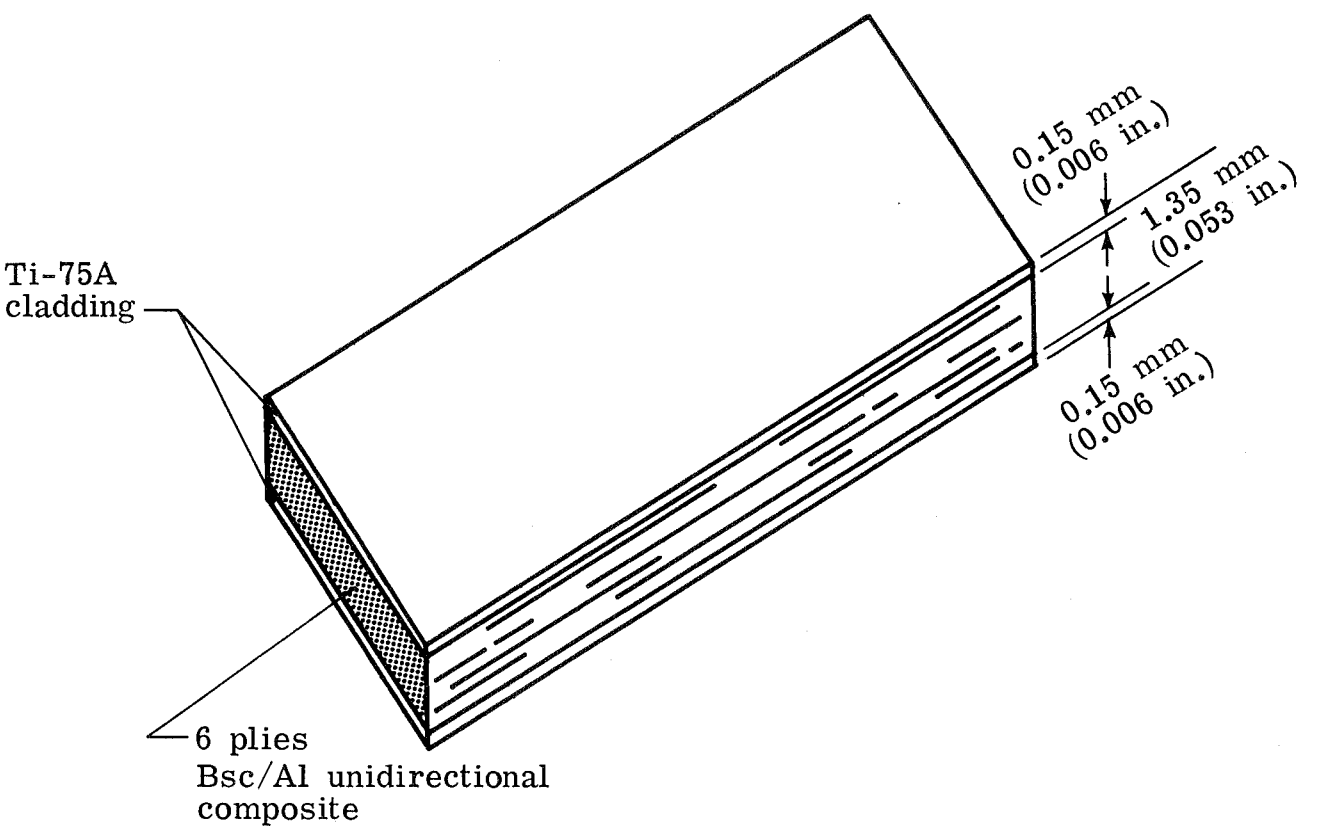

Figure 1.- Schematic diagram of Ticlad Bsc/Al sheet material.

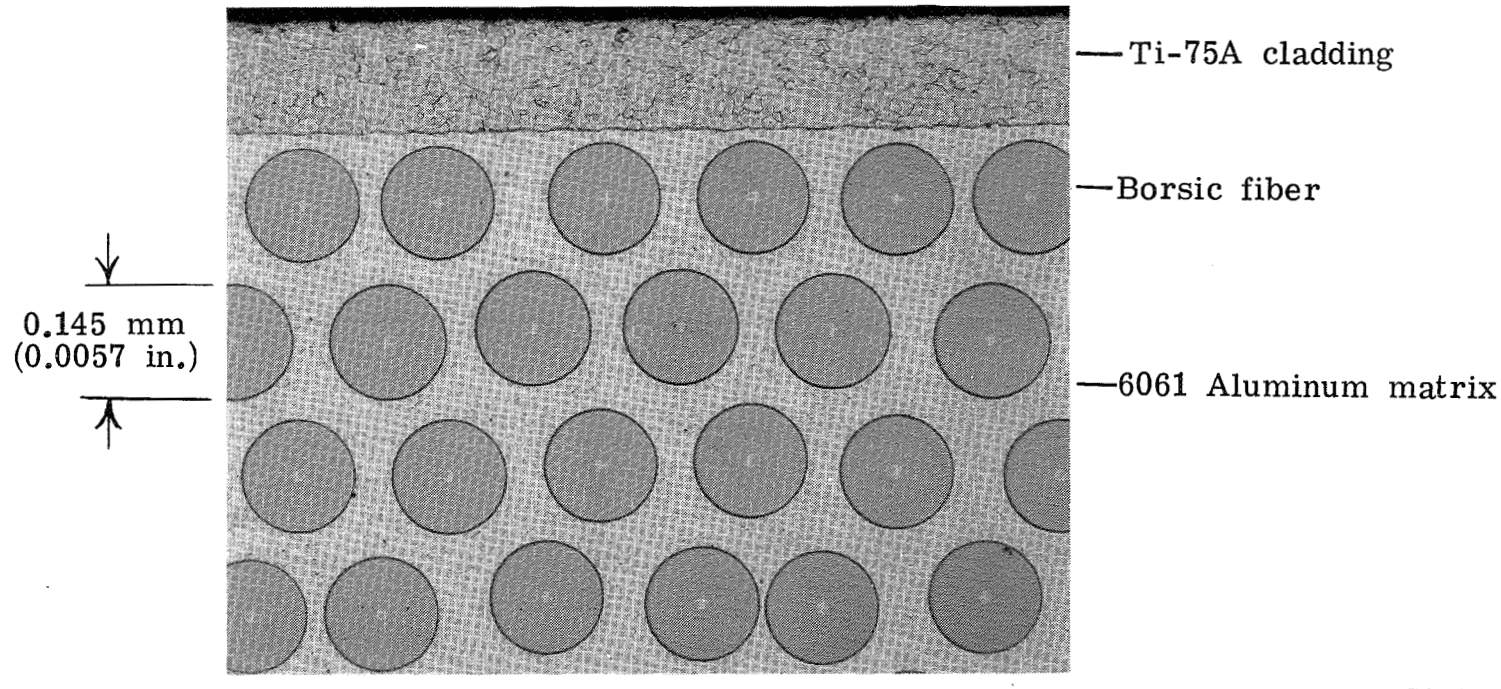

L-79-339

Figure 2.- Cross-section photomicrograph of "as received" Ticlad Bsc/Al sheet material.

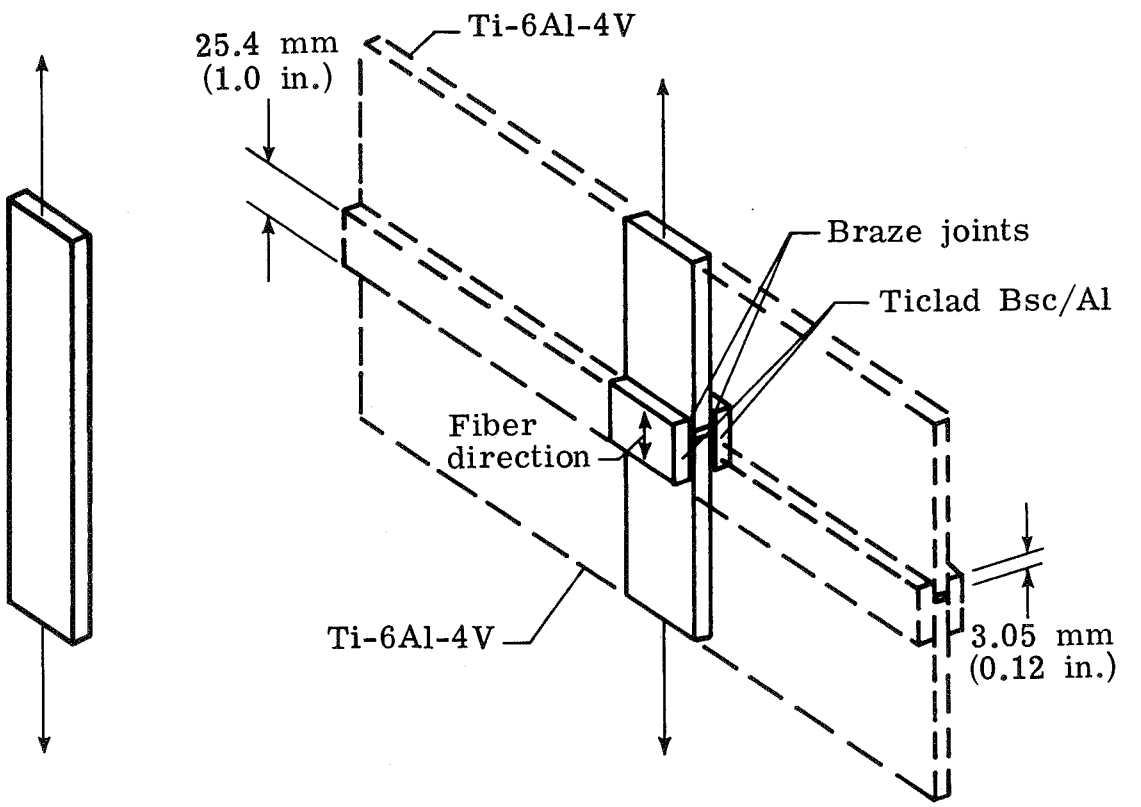

(a) Tensile.

(b) Double-overlap braze joint.

Figure 3.- Schematic diagram of test specimens.

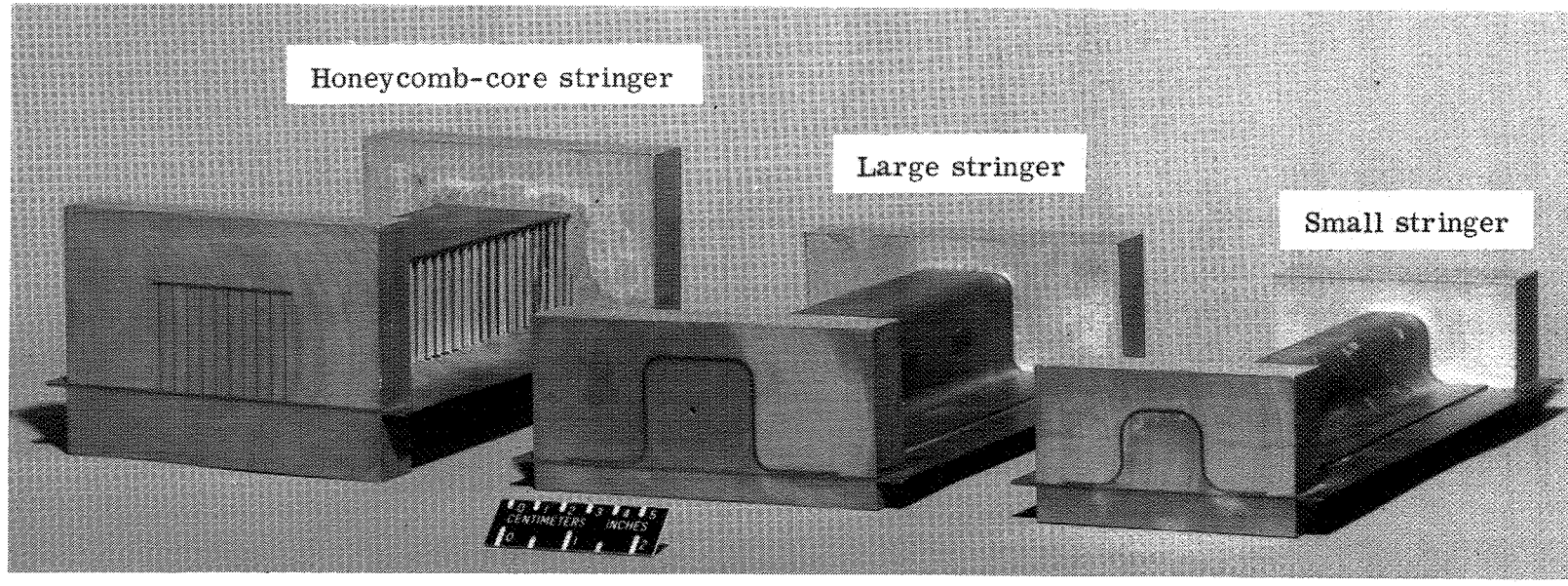

L-78-5948.1

Figure 4.- Typical skin-stringer panels.

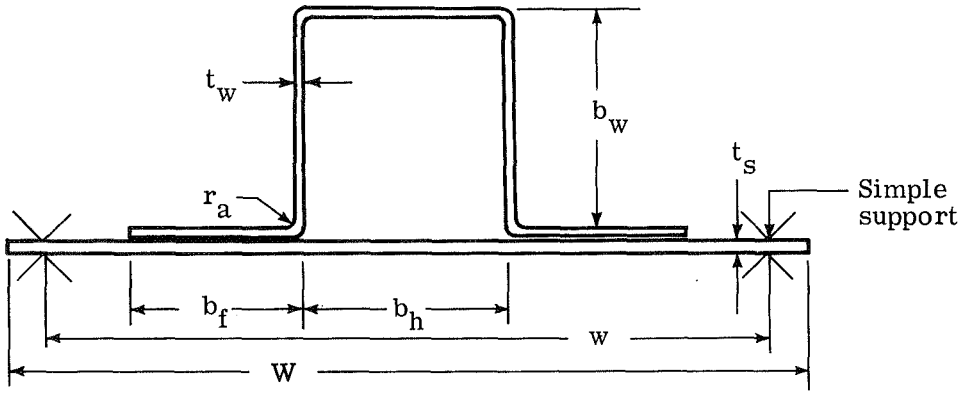

(a) Hat-shaped stringer.

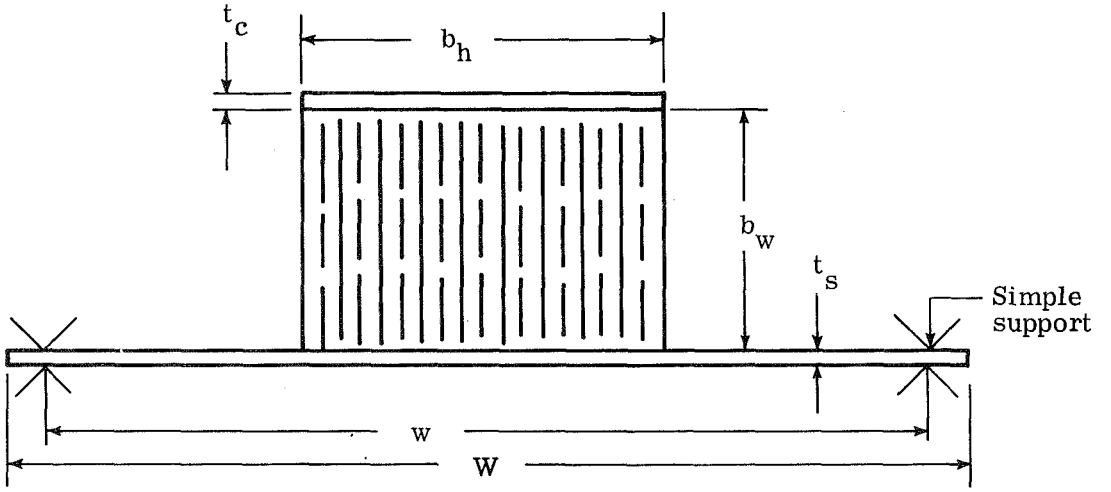

(b) Honeycomb-core stringer.

Figure 5.- Cross sections of skin-stringer panels (see table I for values of dimensions).

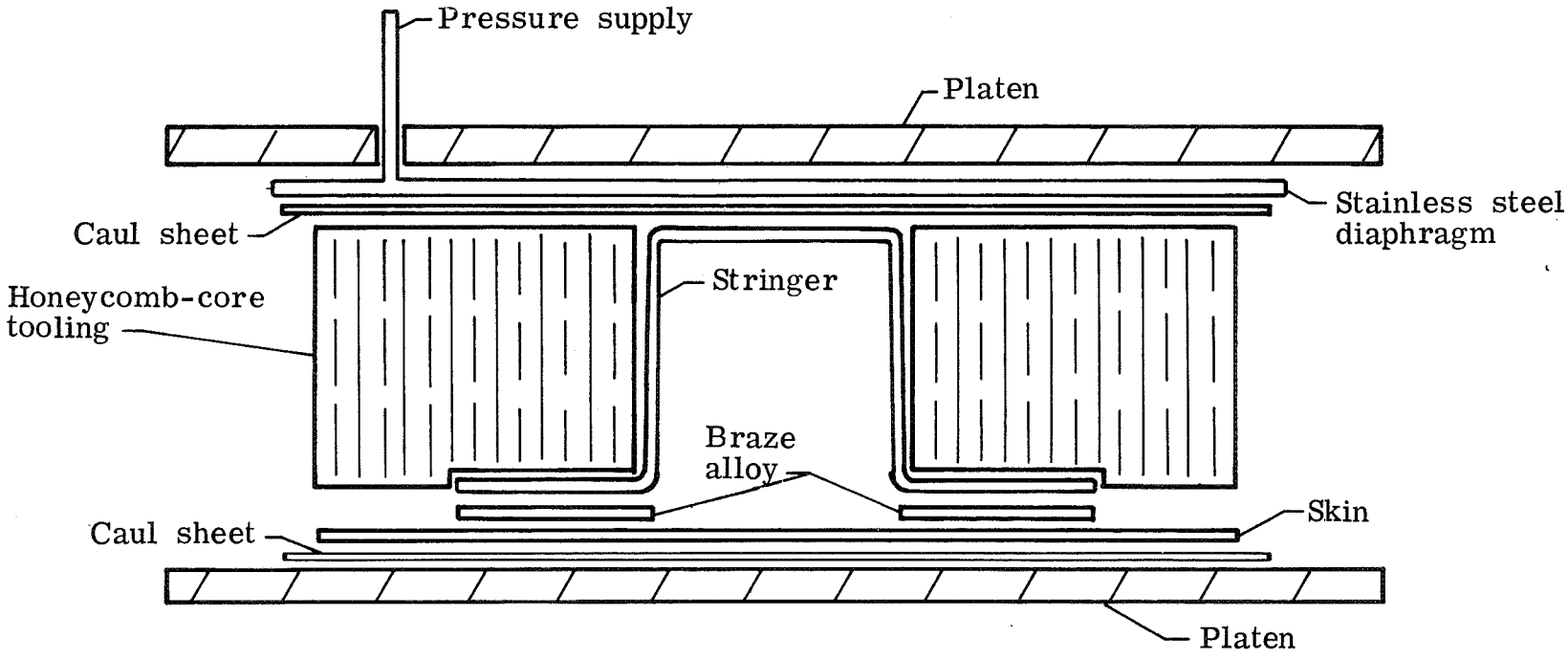

Figure 6.- Cross section of tooling for brazing.

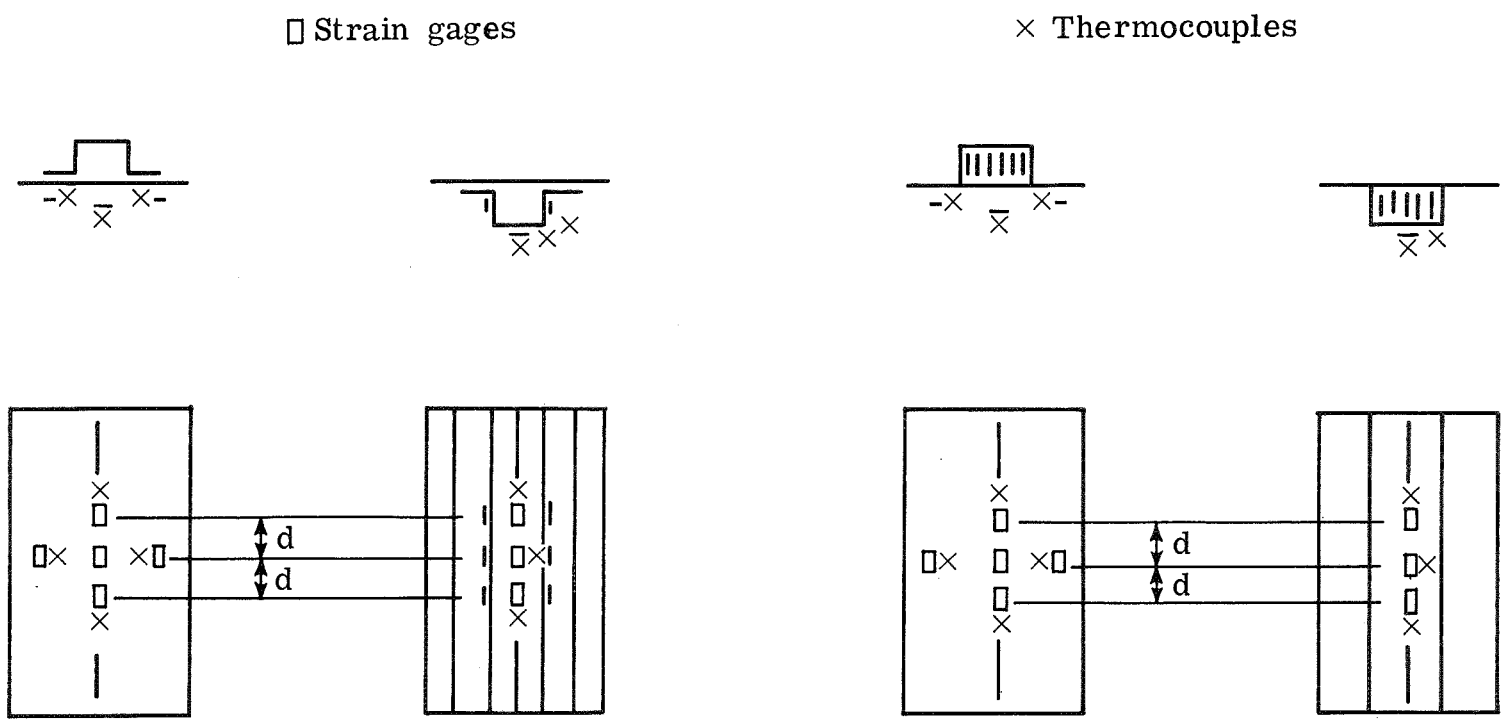

(a) Large (L) and small (S) hat-shaped stringers.

(b) Honeycomb-core stringer (H).

Figure 7.- Locations of strain gages and thermocouples on skin-stringer panels; d = 50.8 mm (2.0 in.) for L and H panels; d = 38.1 mm (1.5 in.) for S panels.

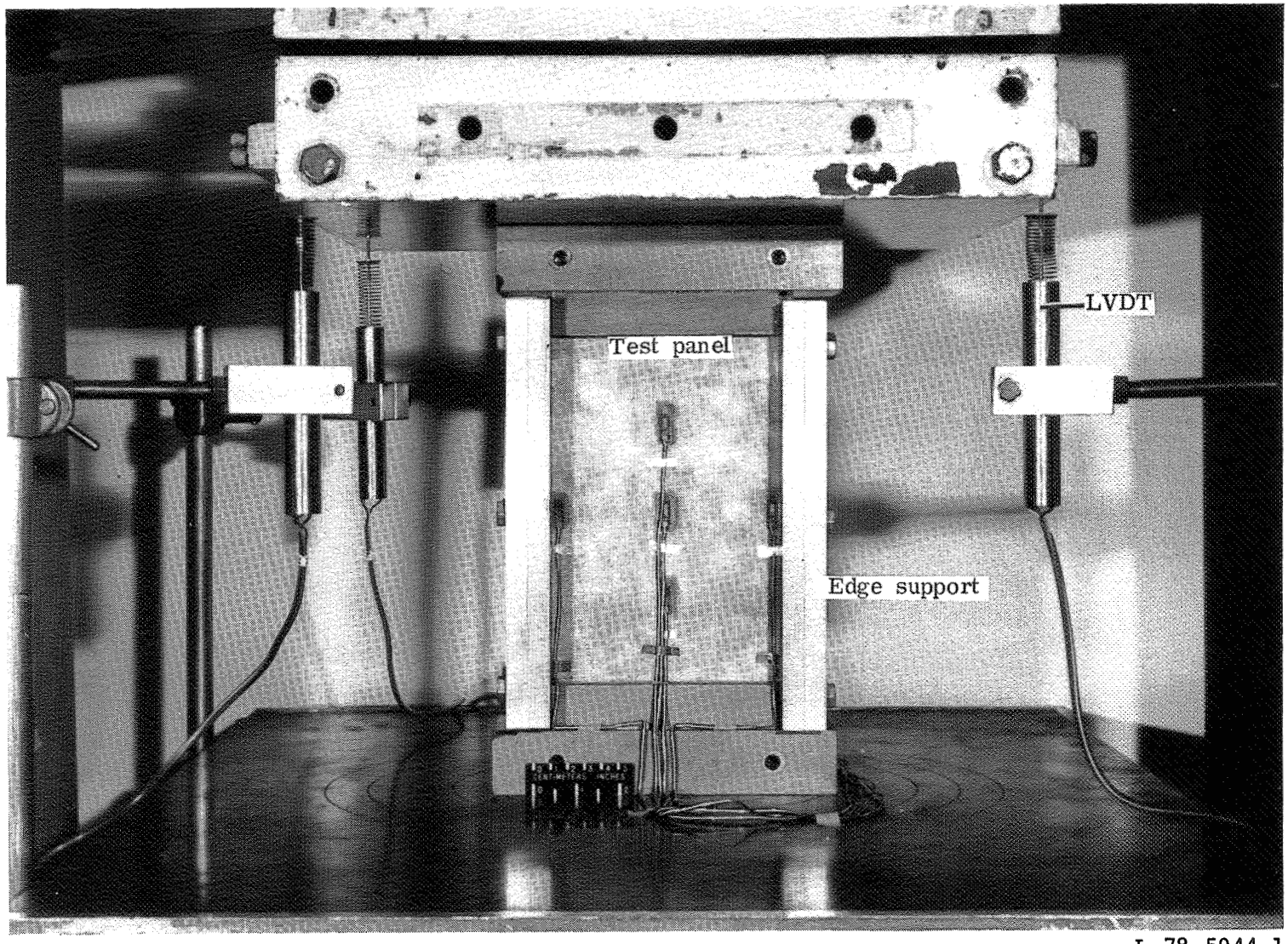

L-78-5944.1

Figure 8.- Room-temperature test setup for skin-stringer panels.

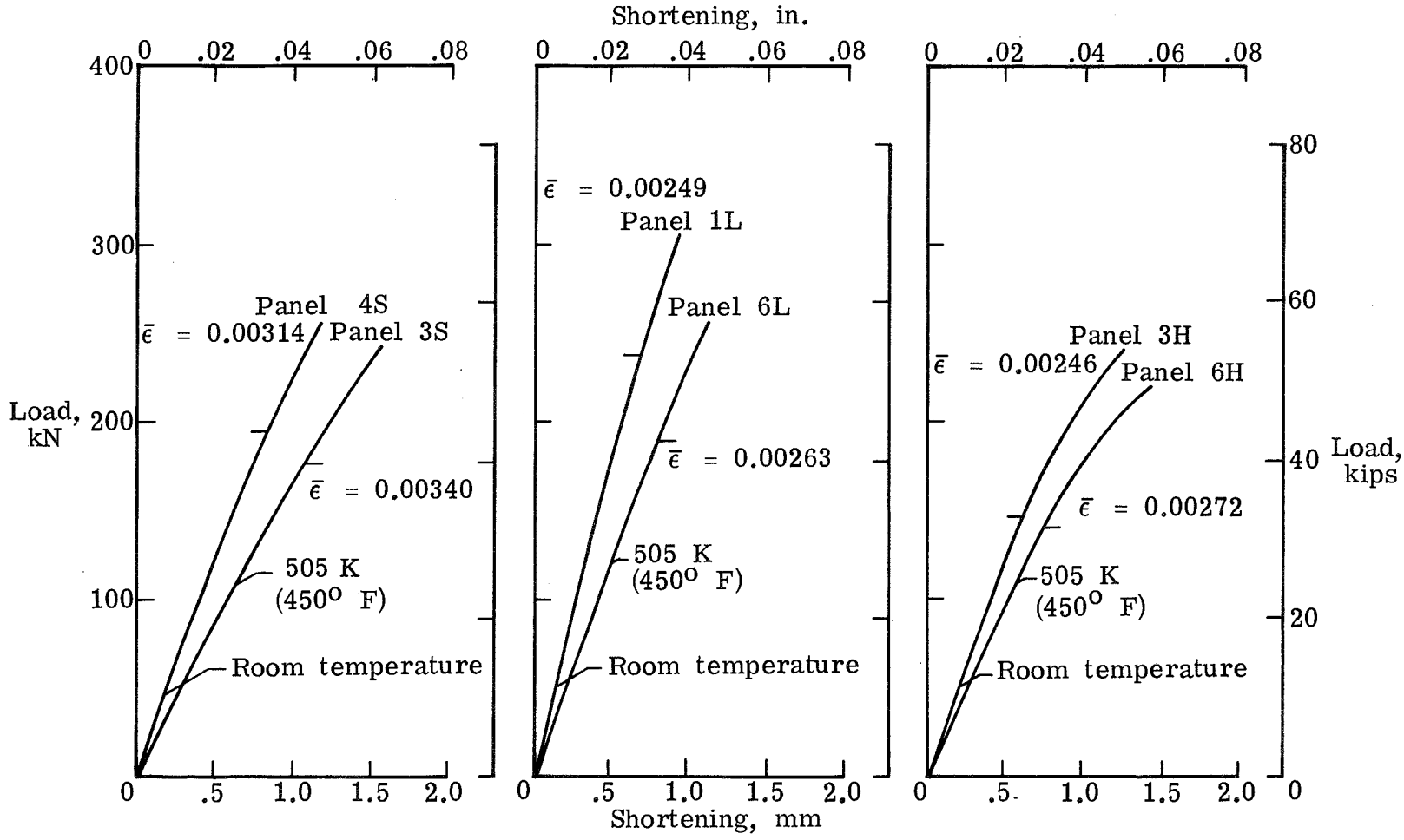

(a) Small stringer (S). (b) Large stringer (L). (c) Honeycomb-core stringer (H).

Figure 9.- Typical LVDT load-shortening curves for skin-stringer panels;
$\bar{\epsilon}$ = Average strain of skin strain gages at strain reversal.

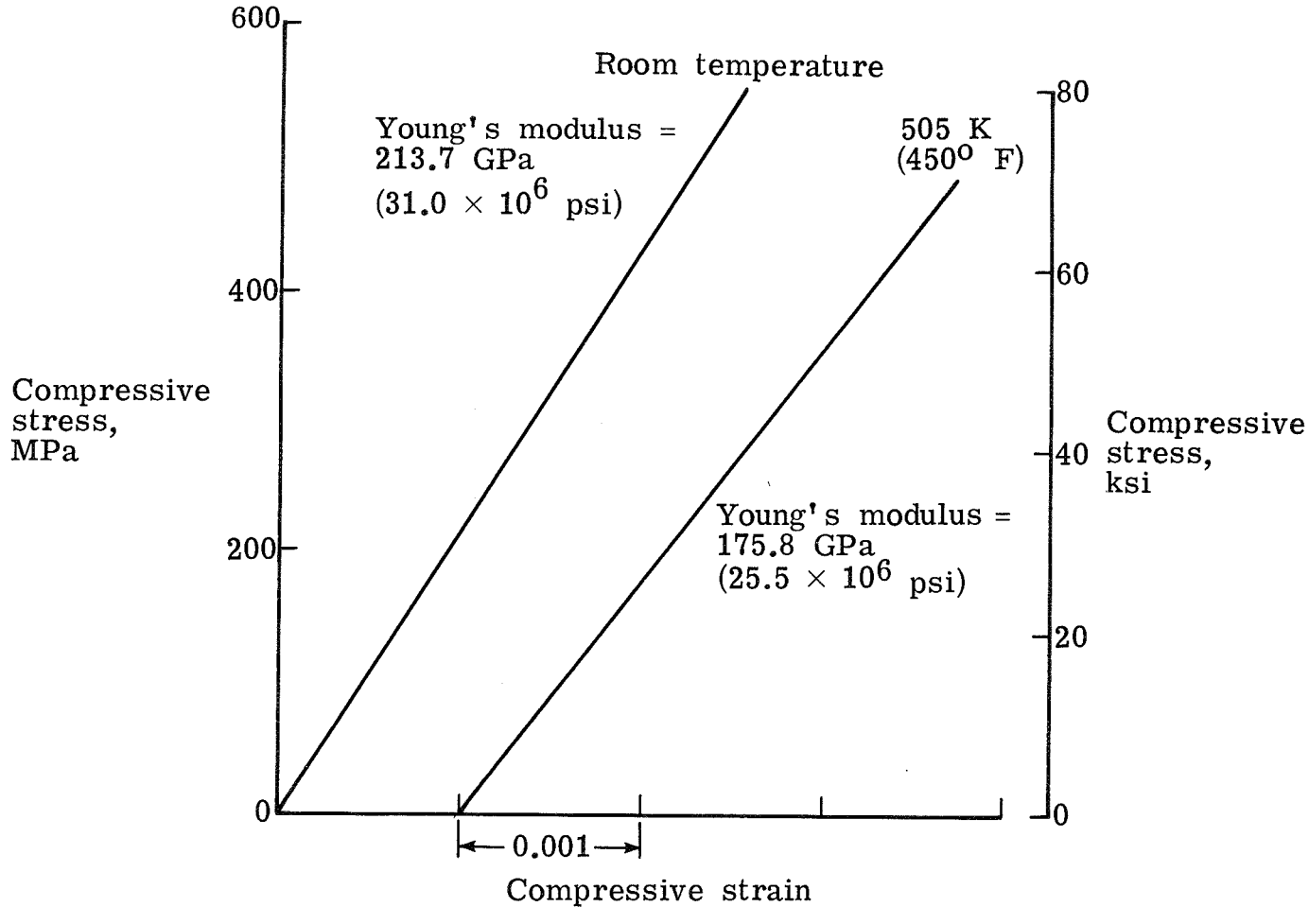

Figure 10.- Compressive stress-strain curves for Ticlad Bsc/Al.

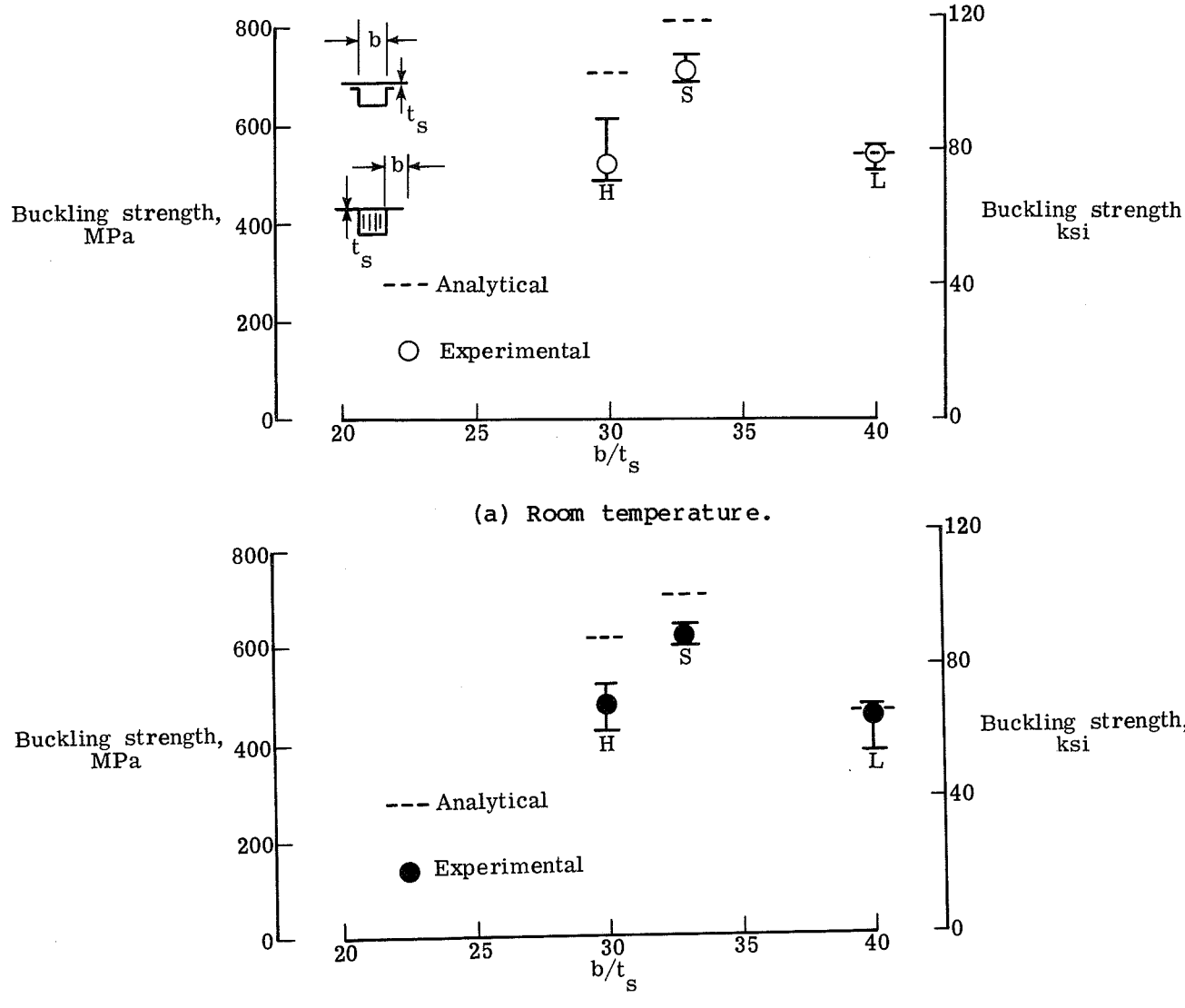

Figure 11.- Comparison of experimental and analytical buckling strengths for large (L) and small (S) hat-shaped stringers and honeycomb-core (H) stringers.

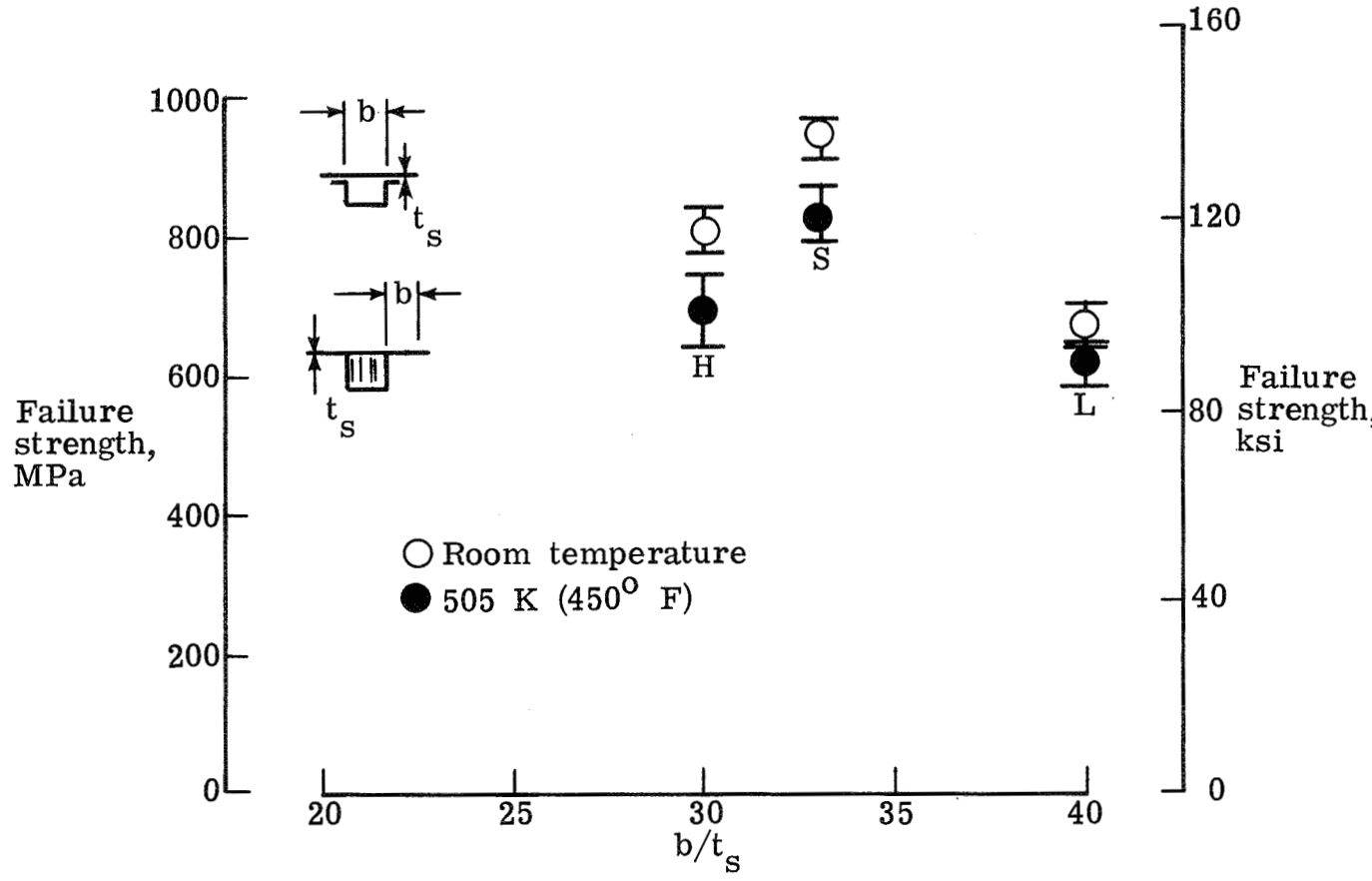

Figure 12.- Average failure strength of panels with large (L) and small (S) hat-shaped stringers and honeycomb-core (H) stringers.

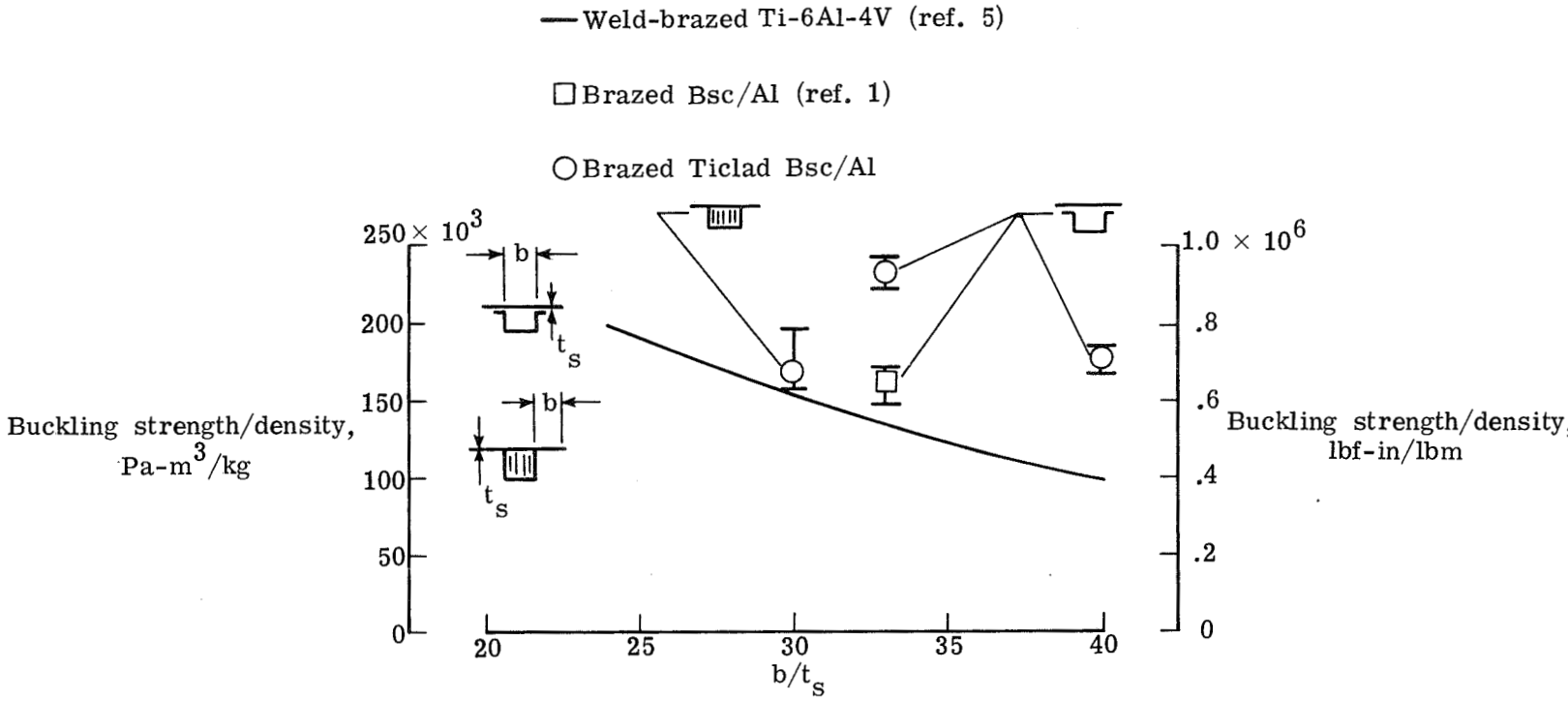

Figure 13.- Comparison of specific buckling strengths of skin-stringer panels.

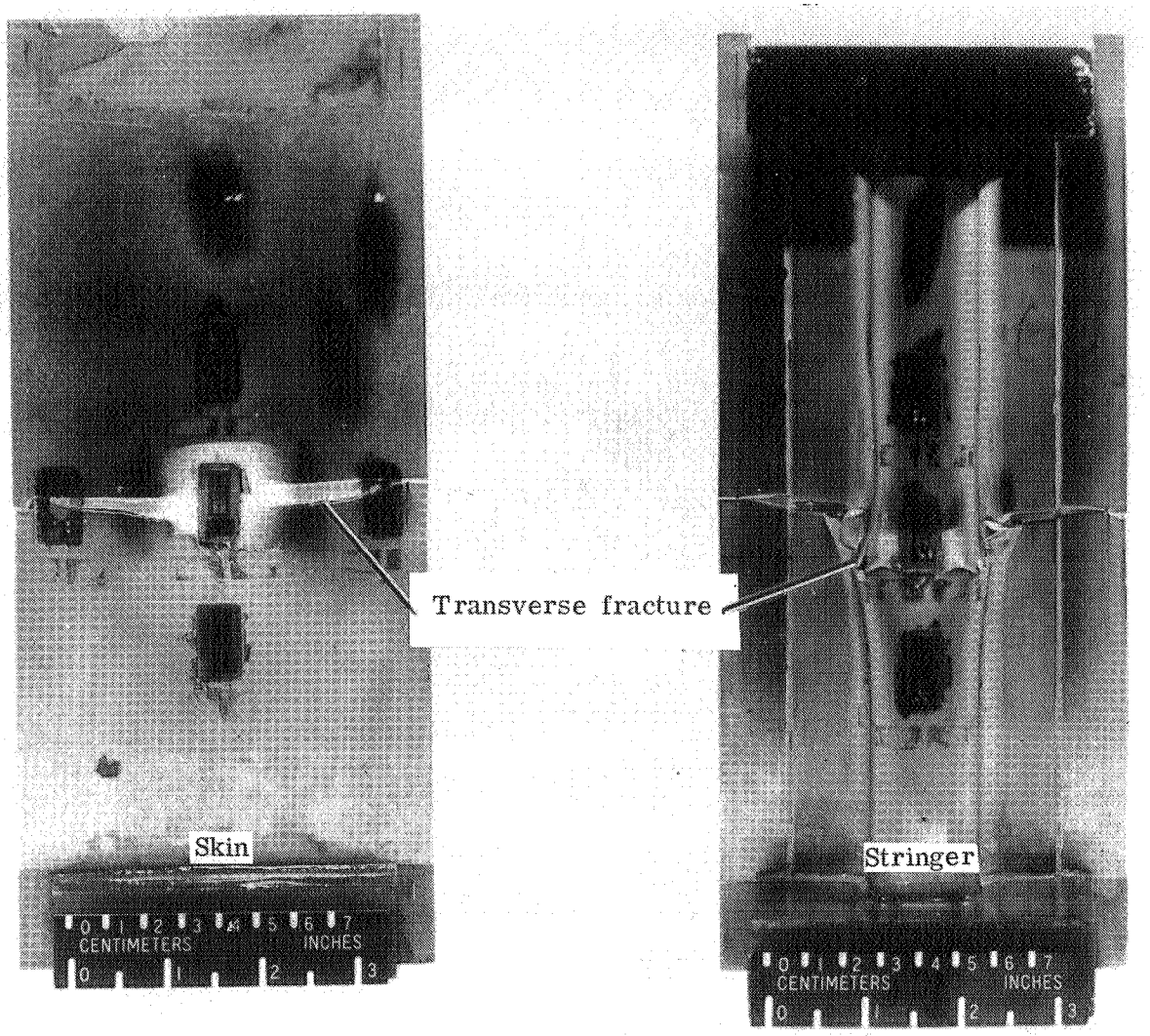

L-79-340

(a) Panel with small stringer.

Figure 14.- Typical failures of skin-stringer panels.

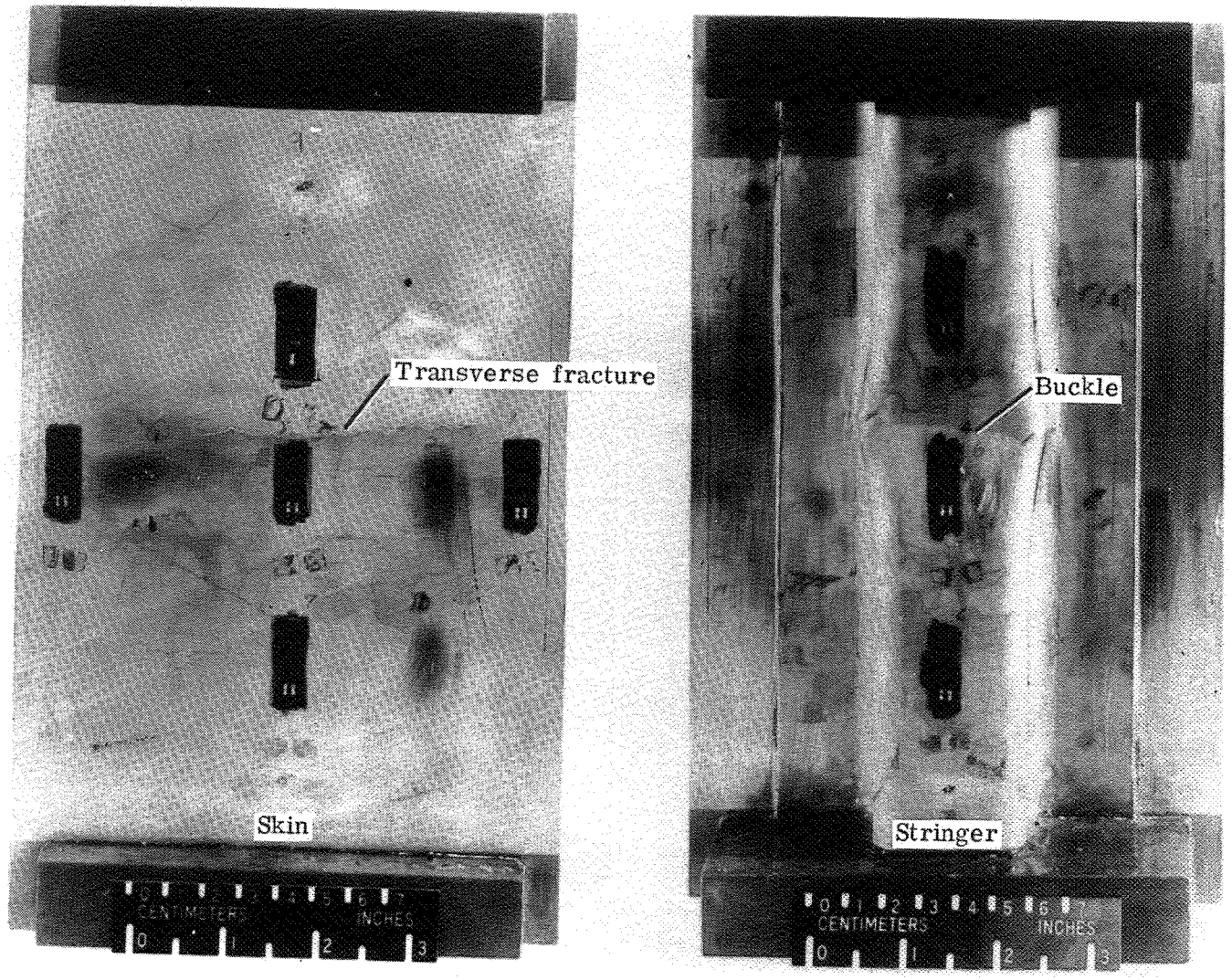

L-79-341

(b) Panel with large stringer.

Figure 14.- Continued.

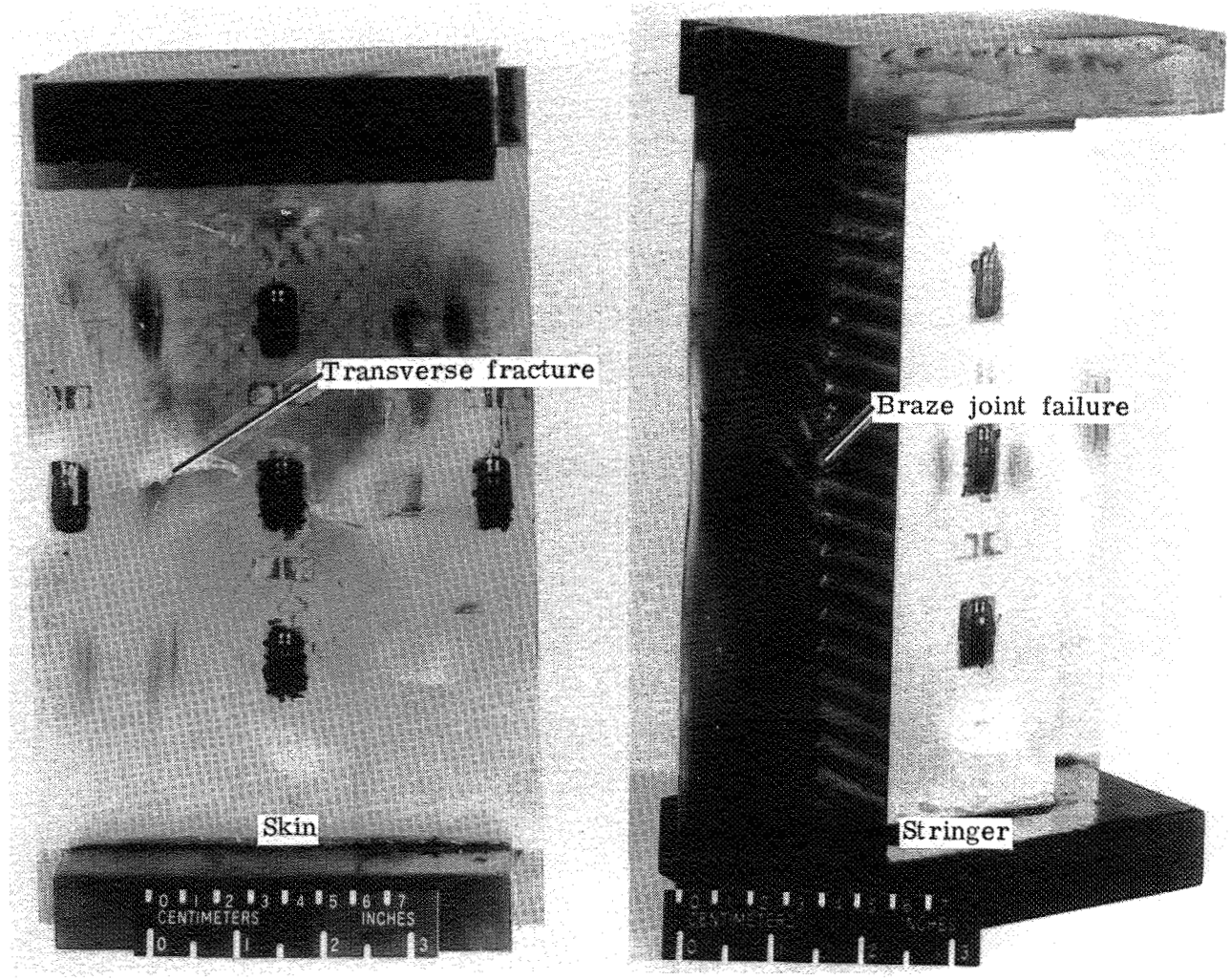

L-79-342

(c) Panel with honeycomb-core stringer.

Figure 14.- Concluded.

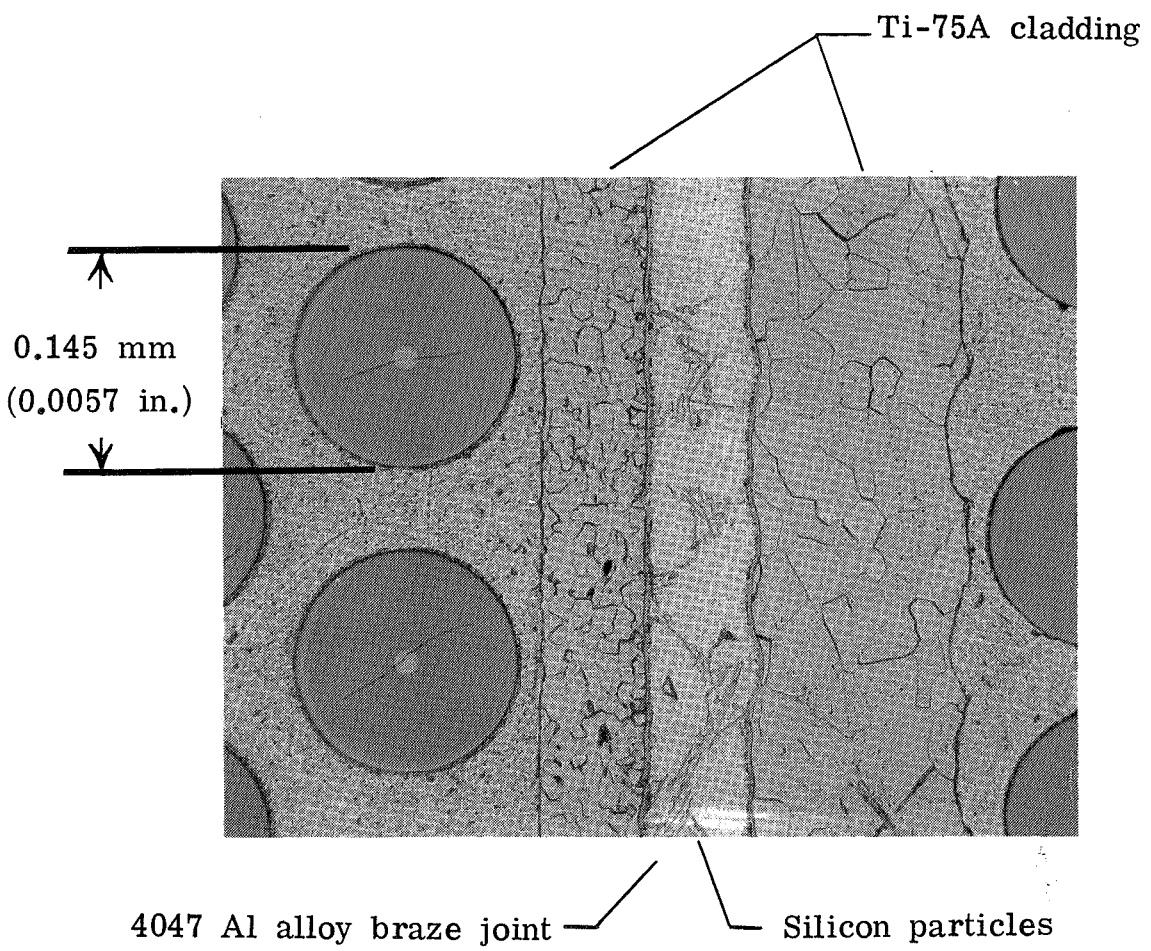

L-79-343

Figure 15.- Typical braze joint for panels with small stringers.

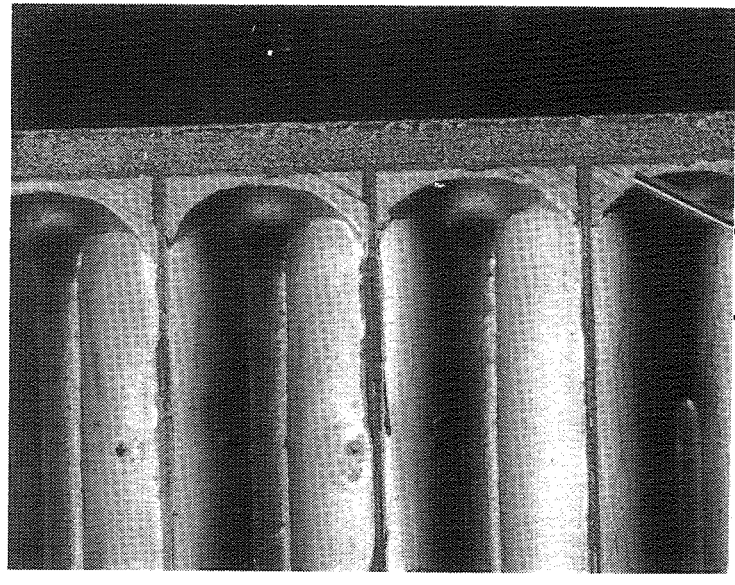

(a) Honeycomb core to skin.

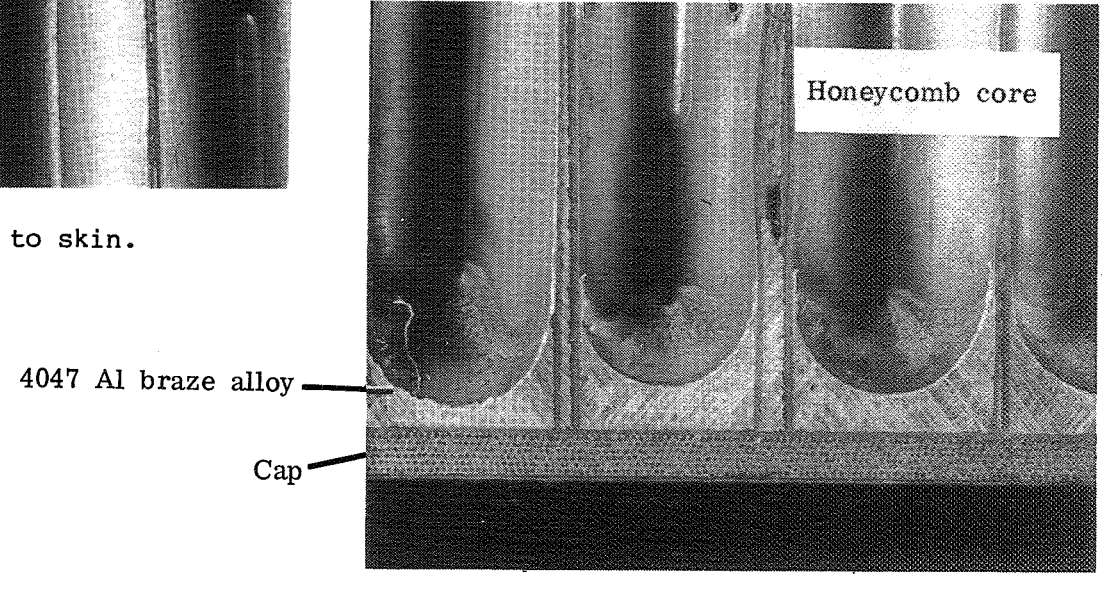

(b) Honeycomb core to cap.

L-79-344

Figure 16.- Photomicrographs of typical braze joints for panels with honeycomb-core stringers.

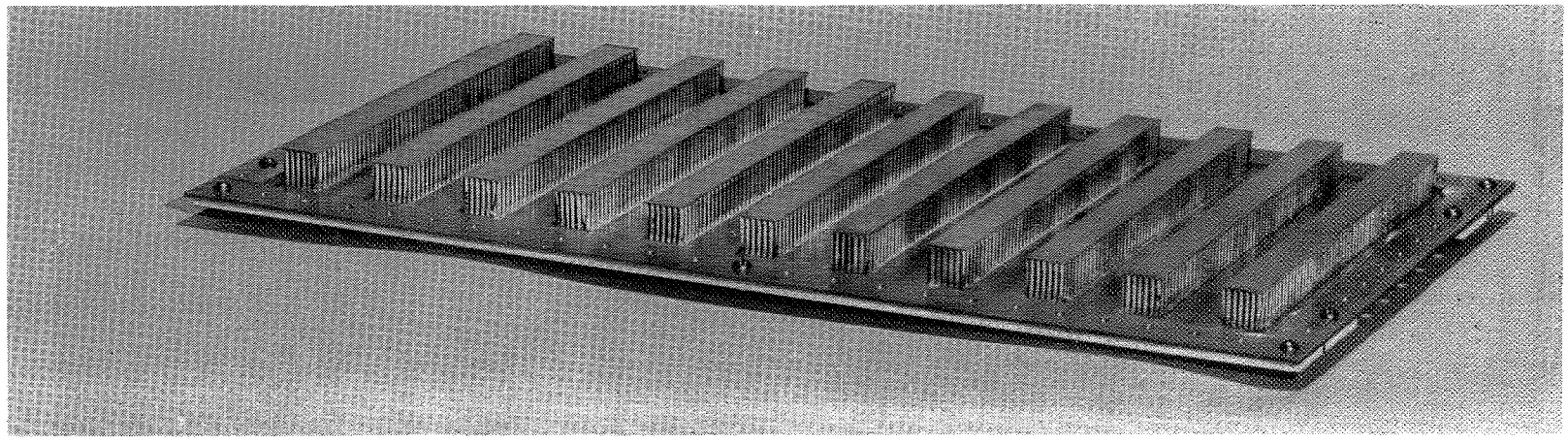

L-77-8658

Figure 17.- A brazed Ticlad Bsc/Al skin-stringer panel for YF-12 aircraft.

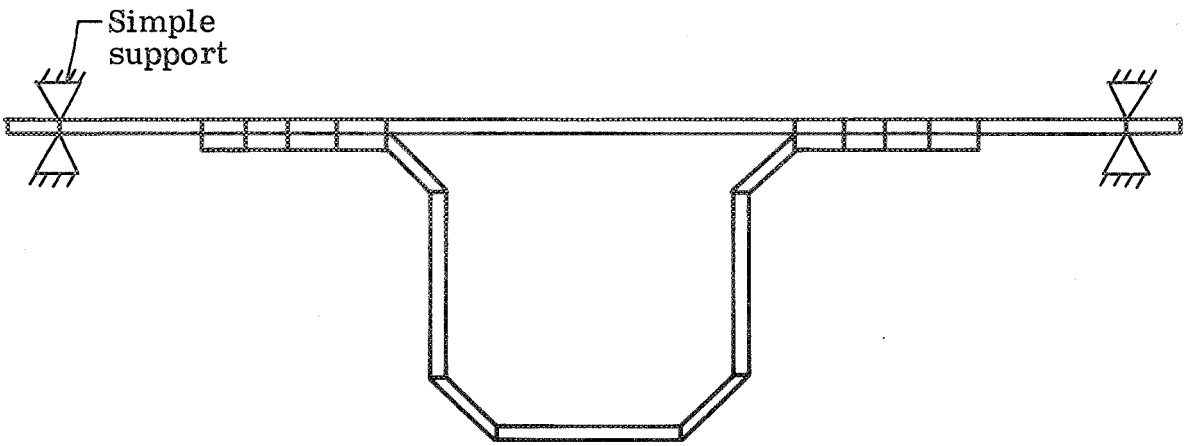

(a) Panels with hat-shaped stringers.

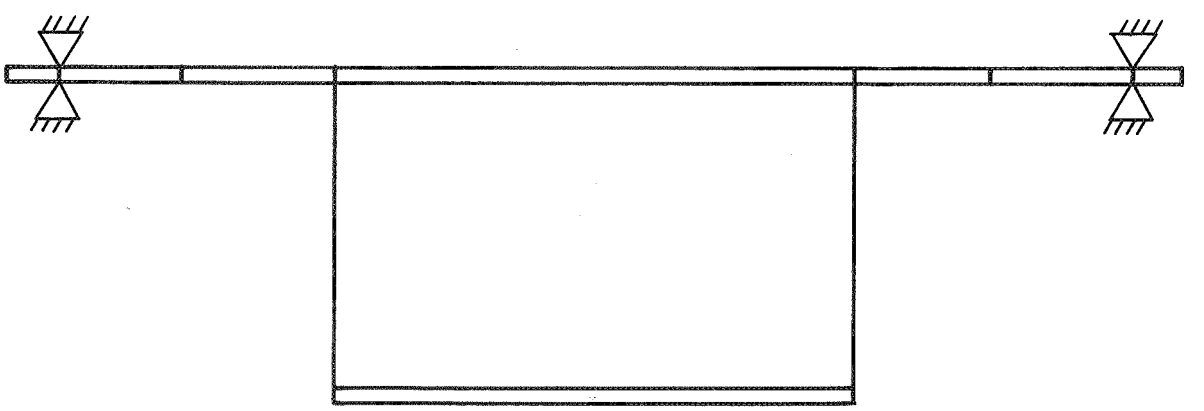

(b) Panels with honeycomb-core stringers.

Figure 18.- VIPASA models used in present analysis.

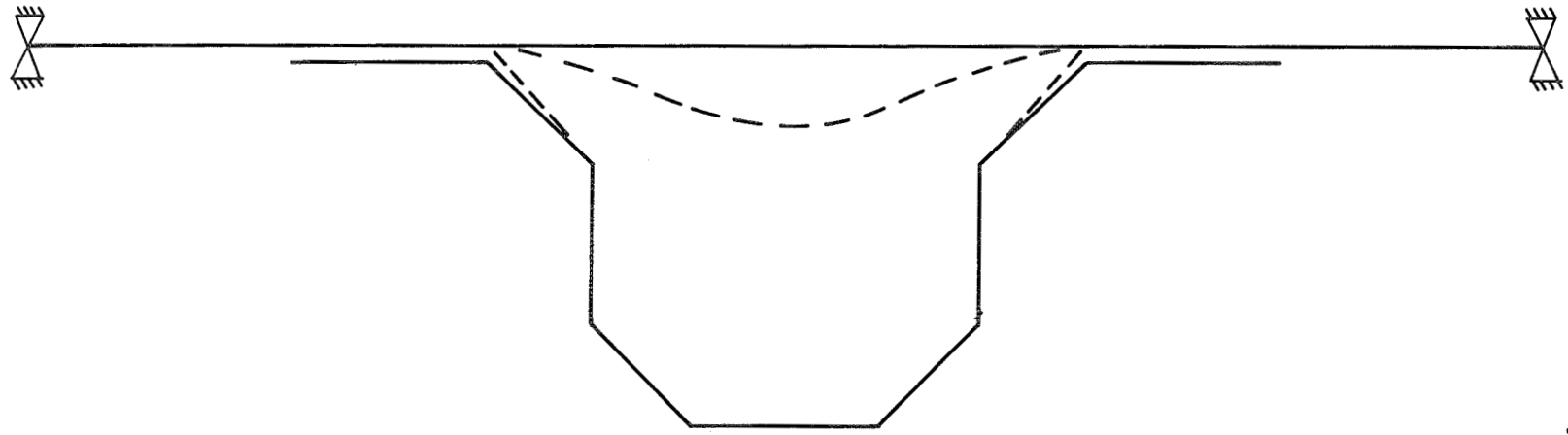

(a) Panel with hat-shaped stringers.

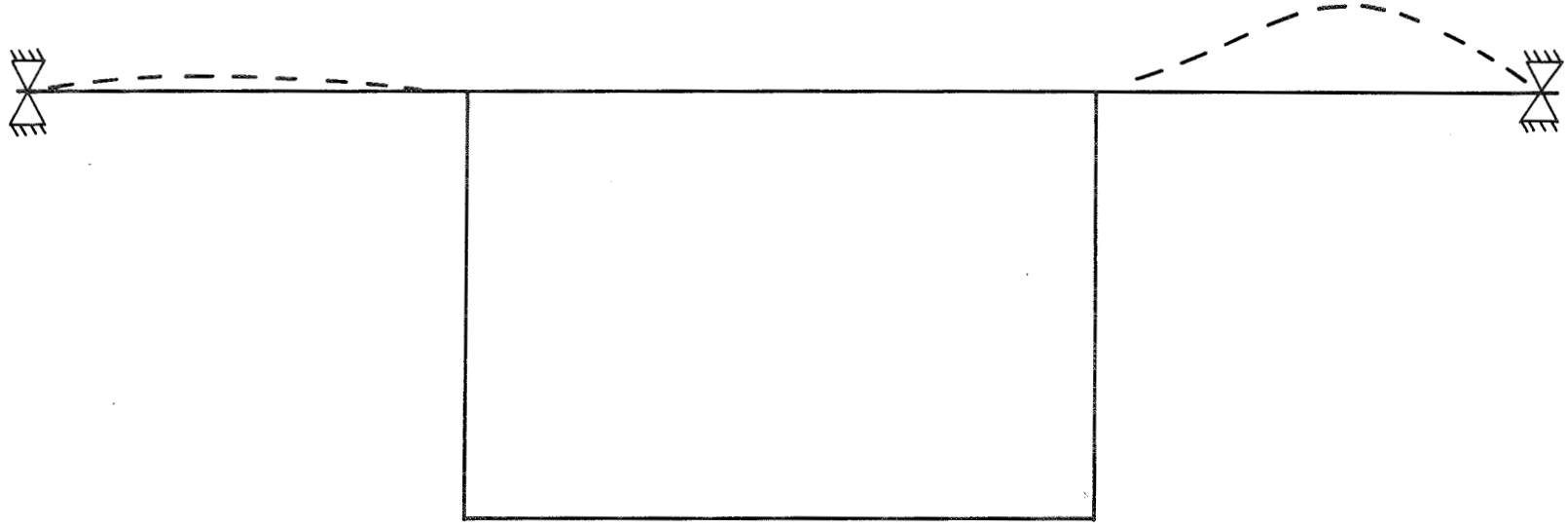

(b) Panel with honeycomb-core stringers.

Figure 19.- Typical mode shape of panel cross sections from VIPASA analyses.

1. Report No. NASA TP-1573	2. Government Accession No.	3. Recipient's Catalog No.
4. Title and Subtitle FABRICATION AND EVALUATION OF BRAZED TITANIUM-CLAD BORSIC®/ALUMINUM COMPRESSION PANELS		5. Report Date March 1980 6. Performing Organization Code
7. Author(s) Dick M. Royster, Robert R. McWithey, and Thomas T. Bales		8. Performing Organization Report No. L-13112 10. Work Unit No. 533-01-13-01
9. Performing Organization Name and Address NASA Langley Research Center Hampton, VA 23665		11. Contract or Grant No. 13. Type of Report and Period Covered Technical Paper
12. Sponsoring Agency Name and Address National Aeronautics and Space Administration Washington, DC 20546		14. Sponsoring Agency Code

15. Supplementary Notes

VIPASA computer analysis described in the appendix was performed by Gerald G. Weaver, Graduate Student at the University of Delaware.

16. Abstract

Processes for brazing Borsic/aluminum composite materials that eliminate diffusion of braze alloy constituents into the aluminum maxtrix have been developed at the NASA Langley Research Center. One brazing study led to the development of a hybrid composite which combines high strength Borsic/aluminum and ductile titanium to form a material identified as titanium-clad Borsic/aluminum. The titanium foil provides the Borsic/aluminum with a durable outer surface and serves as a diffusion barrier which alleviates fiber and matrix degradation during brazing. Titanium-clad Borsic/aluminum skin panels were joined to titanium-clad Borsic/aluminum stringers by brazing and were tested in end compression at room and elevated temperatures. The data include failure strength, buckling strength, and the effects of brazing on the material properties. Predicted buckling loads are compared with experimental data.

17. Key Words (Suggested by Author(s))	18.
Borsic/aluminum Titanium Brazing Skin-stringer panels Material properties	

19. Security Classif. (of this report)	20. Security Classif. (of this page)	21. No. of Pages	22. Price
Unclassified	Unclassified	40	

NASA-Langley, 1980